Energy 342 (2026) 139598

Contents lists available at ScienceDirect

Energy

journal homepage: www.elsevier.com/locate/energy

Numerical perspective of copper nanoparticle morphology on energy conversion in a novel photovoltaic-thermal system

Yassine El Alami [a,*], Elhadi Baghaz [a], Mohamed Errebii [b], Rehena Nasrin [c], Mohamed El Habib Amagour [d], Khaled M. Al-Aribe [e], Adnan Ibrahim [f,**]

[a] Laboratory of Electronics, Instrumentation and Energetic, Faculty of Sciences, Chouaïb Doukkali University, El Jadida, Morocco
[b] LPMAT Laboratory, Department of Physics, Faculty of Sciences Ain Chock, Hassan II University, Casablanca, 20100, Morocco
[c] Department of Mathematics, Bangladesh University of Engineering and Technology, Dhaka, 1000, Bangladesh
[d] Green Energy Park, IRESEN-UM6P, Km 2 Route Régionale R206, Benguerir, Morocco
[e] Department of Mechanical and Industrial Engineering, Abu Dhabi University, Abu Dhabi, PO Box 59911, United Arab Emirates
[f] Solar Energy Research Institute, Universiti Kebangsaan Malaysia, Bangi, Selangor, 43600, Malaysia

ARTICLE INFO

Keywords:
Photovoltaic-thermal systems
Copper nanoparticles
Nanofluids
Energy and exergy efficiency
Three-dimensional numerical simulation

ABSTRACT

The photovoltaic modules' (PV-M) temperature increase significantly reduces their efficiency and accelerates their degradation, highlighting the need to design more efficient and durable photovoltaic-thermal hybrid systems (PVT-Ss). A new PVT-S, evaluated through three-dimensional numerical modeling in COMSOL Multiphysics, is recommended, which analyzes several criteria varying inlet velocity and solar radiation, including energy-exergy efficiency, durability, annual production, exergy destruction, and entropy generation phenomena. Two working fluids were compared: clear water and a nanofluid based on copper nanoparticles (Cu NPs) dispersed in water. Different forms of these nanoparticles were tested to identify the optimal configuration. The results show that blade-shaped nanoparticles offer the best performance, with a 3.21 % improvement in thermal efficiency compared to octahedron-shaped nanoparticles and a 3.56 % improvement compared to cooling using water alone. The maximum exergy efficiency of 15.35 % is obtained for PVT-S using Cu/water nanofluid, compared to a 15.13 % value achieved for PVT-S using pure water at low velocity. The total annual energy-exergy productions for PVT-S using Cu/water are 2672.09 kWh and 515.76 kWh, respectively. These values are higher than those obtained for PVT-S using pure water and for the conventional PV-M. The sustainability of the system improves as solar irradiance increases, reaching a value of 1.1689 for the PVT-S based on the Cu/water nanofluid. The findings of this work reveal that the use of Cu NP-based nanofluids, combined with geometry optimization, maximizes the energy and exergy efficiencies of the PVT-S while enhancing its overall sustainability.

Nomenclature

Abbreviations			
TEF	Thermal efficiency	$\dot{X}_{sun}$	Exergy solar radiation on PVT system
BC	Boundary condition	T_{out}	Output water temperature (°C)
SI	Sustainability index	n	Surface normal
PV-M	Photovoltaic module	$\dot{X}_{des}$	Exergy destruction of the PVT system
TPT	Tedlar-polyester-Tedlar	q	Heat flow vector

(continued on next column)

(*continued*)

EEF	Electrical efficiency	$\dot{X}_{el}$	Electrical exergy (W)
MFRT ($\dot{m}$)	Mass flow rate	T_c	Solar cell temperature (°C)
EVA	Acetate ethylene vinyl	$\dot{m}$	Mass flow rate (kg/s)
FEM	Finite element method	$\dot{X}_{th}$	Thermal exergy (W)
Cu	Copper	A_{th}	Area of the collector (m^2)
PVT-S	Photovoltaic-thermal system	d_g	Annual degradation rate
Parameters		u, v, w	Velocity components (m/s)

(continued on next page)

* Corresponding author.
** Corresponding author.
E-mail addresses: yassineelalami97@gmail.com (Y. El Alami), iadnan@ukm.edu.my (A. Ibrahim).

https://doi.org/10.1016/j.energy.2025.139598
Received 30 October 2025; Received in revised form 23 November 2025; Accepted 8 December 2025
Available online 10 December 2025

(*continued*)

G_t	Annual solar irradiance (kWh/m^2/day)	$\dot{S}_{gen}$	Entropy generation in the PVT system
T_{ted}	Tedlar temperature (°C)	d_{ge}	Annual model degradation (%)
A_{PVT}	PVT area (m^2)	E_{el}	Electrical power (W)
P_c	Packing factor (%)	**Greek Symbols**	
v_{in}	Input velocity (m/s)	μ	Viscosity (Pa.s)
Q_{th}	Thermal energy (W)	η_{el}	Electrical efficiency (%)
Ts	Surface temperature, (°C)	ρ	Density (kg m^{-3})
k	Thermal conductivity (W m^{-1} K^{-1})	ε_{th}	Exergy efficiency (thermal) (%)
C_p	Specific heat (J kg^{-1} K^{-1})	η_{th}	Thermal efficiency (%)
T_g	Glass temperature (°C)	ε_{PVT}	Exergy efficiency (total) (%)
E_{abs}	Received energy (W)	ε_{el}	Exergy efficiency (electrical) (%)
T_{in}	Inlet temperature (°C)		

1. Introduction

The rapid growth of energy demand, together with the negative impact of greenhouse gases on the climate, has led the scientific community to rethink traditional energy production methods [1]. Fossil fuels, long considered the main energy source, are no longer able to meet current environmental and sustainability challenges. This has shifted research attention toward renewable energy, especially solar energy, which is abundant and has a low ecological footprint [2,3]. Among the available technologies, silicon-based PV-Ms are particularly important because they can directly convert sunlight into electricity. However, they also have limitations. Typically, around 80 % of the incoming solar radiation is absorbed, but less than a quarter is converted into electrical energy. The remainder is lost as heat, causing cell temperatures to rise above 40 °C, which reduces both efficiency and long-term performance [4].

To reduce these losses, various cooling techniques have been developed. Active methods use pumps or fans to circulate heat transfer fluids, while passive methods rely on natural mechanisms such as air convection or the use of phase-change materials. More recently, hybrid solutions that combine both approaches have been introduced [5], aiming to take advantage of the strengths of each method. It is in this context that PVT-S technology has been developed [6]. By coupling a thermal collector with a PV-M, PVT-Ss can simultaneously generate electricity and useful heat, offering an effective way to enhance solar energy utilization and tackle current energy and environmental challenges.

Numerous studies have focused on optimizing and evaluating the performance of PVT-Ss and PV-M. Variyenli et al. [7] studied a water-cooled PVT-S with a flat-surface elliptical cooling tube to improve heat transfer between the PV-M and the tubes. Experimental tests and numerical simulations showed that the designed PVT-S achieves a maximum electrical efficiency (EEF) of 17.57 % and an overall efficiency of 69.38 %, surpassing conventional PV-M (16.13 %), with an average deviation of 3.2 % between experimental and numerical results, demonstrating the design effectiveness to improve thermal-electrical performances. El Alami et al. [8] suggested a simplified, lightweight PVT-S to overcome the limitations of conventional systems. Their study evaluated the number of holes and fluid thickness effects on energy-exergy efficiency and pressure drop. The configuration with a thin liquid layer of 1 mm showed the best performance, with an EEF, TEF, and total exergy efficiency of 13.76 %, 79.80 %, and 15.96 %, respectively. But pressure losses were higher (848–875 Pa). Satpute et al. [9] compared rectangular and circular spiral PVT-S absorbers with water as the heat transfer fluid. The rectangular coil showed the best performance, with an EEF of 14.32 % and a TEF of 63.56 %, reducing the temperature of the cells and outperforming the circular coil and PV-M without an absorber, with good agreement between experimental and numerical results. Wang et al. [10] analyzed several PVT-S configurations to optimize heat transfer and electrical performance, studying the influence of collector material, irradiation, mass flow rate (MFRT), and inlet temperature. The cylindrical structure increased EEF by 1.73 % and TEF by 8.29 %, with aluminum identified as the most cost-effective material. Jha et al. [11] compared a PVT-S with a trapezoidal plate to a conventional unit with a flat plate. The trapezoidal plate reduced the PV-M temperature by 2.8 °C, increased the outlet temperature by 1.9 °C, and decreased exergy destruction by 1.89–2.73 %. It also improved overall annual energy by 8.7 %, overall exergy by 8.4 %, and net electrical energy by 1.62 %, while reducing energy payback time by 5.4–9.5 % and increasing annual CO_2 mitigation by 8.6–8.8 % compared to the conventional unit. El Alami et al. [12] proposed an innovative PVT-S without an absorber plate, allowing direct contact between the water and the PV cells to reduce cost, weight, and pressure drop. Parametric analysis showed that the best configuration, with a side inlet, a collector height of 30 mm, and a water layer of 1 mm, achieves a TEF of 81.27 %, an EEF of 13.76 %, and an overall exergy efficiency of 16.51 %. Increasing the water MFRT improves the annual CO_2 reduction by 1.02 t, with a 28 % increase in environmental cost and a slight decrease in the sustainability index of 0.025. Basalike et al. [13] studied a laminar roll PVT-S with an innovative hexagonal grid channel coupled to a coil, modeled in 3D for its evaporator and condenser functions. The results showed that this configuration optimizes the microchannels' temperature difference and pressure drop, achieving an EEF of 17.56 %, a TEF of 9.25 %, and a maximum refrigerant coefficient of performance of 4.64. Over 15 years, the system would reduce energy costs and CO_2 emissions. In this regards, Liu et al. [14] developed a biomimetic PVT-S collector inspired by leaf veins for improving cooling and temperature uniformity. They found that optimizing design parameters (such as inlet MFRT, channel diameter, bifurcation angle, and number of branches) can reduce the average temperature by 0.6 K, decrease flow resistance by 83.2 Pa, and improve thermal uniformity, offering an innovative approach for high-performance PVT-Ss. In the same direction, Kumar et al. [15] experimentally investigated a PVT-S collector in India for evaluating its electrical, thermal, and exergetic performance under different climatic conditions. Many parameters as water temperature, ambient air temperature, and solar radiation measurements were utilized for analyzing the overall efficiency of this system. And their results confirmed that combined heat and power generation improves overall energy utilization and supports the practical deployment of PVT-Ss. On the other hand, Almadhhachi et al. [16] developed a modified PVT-S that incorporate a transparent sheet for reducing heat loss. Their numerical study showed that this modification can improve the overall efficiency of the collector, stabilize performance in the face of environmental variations, and optimize heat transfer, which makes the system particularly suitable for cold climates. Recently, El Alami et al. [17] experimentally and numerically compared an uncooled PV, a partially cooled PVT-S, and a thoroughly cooled PVT-S regarding energy and exergy performance. Their findings revealed that the thoroughly cooled PVT-S can offer the better performance, with an increase in TEF of up to 77.89 %, a maximum decrease in cell temperature of 7.04 °C, and a minimum improvement in EEF of 0.48 %. Increasing the MFRT enhances performance, and the thoroughly cooled system reduces the return-on-investment time by 3.86 years compared to the partially cooled PVT-S. Çerçi et al. [18] studied an air-cooled PVT-S incorporating NACA 8412 aerodynamic profiles arranged in different positions to improve heat exchange. The study evaluated the influence of geometric parameters and air flow conditions on energy and exergy performance. The best results were obtained with a spacing of 50–70 mm in the flow direction and 35 mm in the transverse direction, while limiting the air velocity to 5 m/s to reduce fan consumption. This configuration optimized heat and electrical transfer, demonstrating the value of aerodynamic fins as heat exchangers in PVT-Ss.

Recently, nanofluids have been widely utilized in such systems due to their ability to lower the temperature of PV-Ms and improve their overall performance. For example, Safarianbana et al. [19] studied a PVT-S using a two-phase thermosiphon with a water/MAX phase nanofluid for rear panel cooling. The nanofluid has high thermal conductivity and low cost compared to MXenes. A concentration of 1 wt% reduced the temperature by 19.9 °C and increased the electrical power by 1.68 W. This configuration improved EEF by 19.63 % compared to conventional PV-M. Jabeen et al. [5] evaluated a PVT-PCM system with and without fins using 3D transient simulation, using water, rGO/water nanofluid, and Ag-rGO/water as fluids. The fins reduced the PV-M temperature by approximately 3 K, increased the liquid fraction of the PCM by 10 % and the energy storage by approximately 52 kJ, thereby improving EEF (up to +1.38 %) but with a slight decrease in the TEF of the fluid (−2.82 %). The Ag-rGO/water nanofluid offered the best thermoelectric performance compared to the other fluids. Madadi and Abbasian [1] developed a PVT-S collector with Cu fins and tubes with PCM (paraffin) attached to the back of the PV, tested with water, SiC/water, and graphene/water (0.2–0.4 %, 0.5–1 L/min). The graphene/water nanofluid offered the best cooling and thermoelectric performance, and increasing the concentration and MFRT further enhanced these gains. Sofiah et al. [20] studied the integration of an hBN/water nanofluid (0.5 % vol.) into an indoor PVT-S. Experimental results showed that the panel temperature was reduced from 63 °C to 39 °C at 380 W/m^2, electrical power increased from 12.03 W to 21.17 W, and heat gain reached 255 W at 780 W/m^2. Exergy efficiency improved to 8.7 %, compared to 5.8 % for water alone. In comparison, exergy losses and entropy generation decreased by 2.9 % and 2.8 %, respectively, highlighting the potential of hBN/water nanofluid to improve the performance and sustainability of PVT-Ss. In this context, Radhi et al. [21] investigated a PVT-S featuring square microfins, micro-fin tubes, and twisted ribbon, employing water and an Al_2O_3 nanofluid at concentrations of 0.1–0.2 % vol., together with enriched PCM at 1 % vol. With this configuration, the cell temperature reduced from 77.8 to 35.7 °C, achieving a TEF of 86.5 %, an EEF of 13.171 % (representing a gain of 39.24 %), and a maximum power of 24.44 W. Similary, Azeez et al. [22] developed an advanced PVT-S that combines dimpled and petal-patterned absorber tubes twisted ribbons and nanofluids embedded in PCM. With this configuration, thermal performance was improved threefold compared with a smooth tube using water alone, leading to a 32 % increase in EEF and to a 21.2 % increase in TEF. The system produced a total energy of 2.11 MWh reduced CO_2 emissions by 0.63 t, thereby demonstrating not only energy efficiency but also economic and environmental viability. Jaber et al. [23] investigated a PVT-S equipped with both internal and external micro-fin absorber tubes and double V-cut twisted ribbons, tested with various fluids and PCMs. The best configuration (with 0.8 % CuO and PCM) achieved an EEF of 12.01 %, a TEF of 83.61 %, and a maximum power output of 26.01 W, confirming the effectiveness of this design in enhancing both electrical and thermal performance. In another study, Prasetyo et al. [24] evaluated a PVT-S with fins and an Al_2O_3/water nanofluid. The addition of fins enhanced heat transfer and lowered the temperatures of the PV cells, achieving a maximum electrical conversion efficiency of 13.39 %. Furthermore, Alsharifi et al. [25] investigated an innovative PVT collector featuring twisted porous inserts within straight cooling tubes, using nanofluids. They demonstrated that optimizing key parameters (i.e., tube diameter, insert porosity, width-to-diameter ratio, and nanofluid MFRT) significantly enhances both EEF by 10.49 % and TEF by 46.78 % compared to conventional designs, achieving a maximum desirability score of 1.0 in multi-objective optimization.

Previous studies have consistently shown that elevated temperatures have a negative impact on both the electrical performance and the long-term durability of PV-Ms. Nonetheless, the majority of investigations have focused primarily on conventional collector configurations, including spiral tubes, rectangular coils, various types of overhangs, and roll-bond collectors. While these traditional designs have numerous inherent limitations. In particular, they often lead to non-uniform temperature distributions across the surface of the panels, fail to fully cover the active PV-M surface, all of which result in a noticeable reduction in thermal efficiency (TEF). Furthermore, although nanofluids have been extensively studied for PV-M cooling, the nanoparticles they contain vary in shape and size, and no study has yet systematically evaluated the impact of these different shapes on thermal and electrical performance. This gap prevents the identification of optimal configurations of nanofluids and collectors capable of maximizing the overall efficiency of PVT-Ss.

In response to gaps identified in the literature, this study introduces a new PVT-S whose performance has never been explored before. The novelty lies in the integration of an innovative micro-heat exchanger combined with the use of Cu nanoparticles of different geometries, which simultaneously optimizes the cooling of PV cells and the overall energy efficiency of the system. The analysis was performed using three-dimensional numerical modeling in COMSOL Multiphysics, allowing for an in-depth evaluation of the impact of variations in irradiance and MFRT on criteria such as energy and exergy efficiency, durability, and annual production, as well as exergy destruction and entropy generation phenomena. Two types of heat transfer fluids, pure water and Cu/water nanofluid, were compared to study their cooling capacity and influence on the overall performance of the system. In addition, the study explores the effect of different Cu nanoparticle geometries to identify the optimal configuration for maximizing the thermal and electrical performance of the proposed system.

2. Methodology

2.1. Structure and description of the PVT model

The design focused on integrating a crystalline silicon PV-M with a heat exchanger, enabling the joint use of electricity and heat from solar radiation (Fig. 1). The device is based on a carefully designed multilayer architecture that captures light energy, converts it into electrical current, and recovers excess heat for improving its overall efficiency. The front surface is made of transparent glass, which allows light to pass via while providing mechanical protection against external damage. Just below, sixty PV cells are arranged evenly with a spacing of 2 mm. Each cell, measuring 156.75 × 156.75 mm^2, is interconnected by Cu ribbons forming a continuous electrical circuit [8,12,26,27]. In order to guarantee the module's durability and stability, the cells are encapsulated in a layer of ethylene vinyl acetate (EVA). This provides insulation against moisture and helps maintain long-term performance. The rear side is covered with a Tedlar-Polyester-Tedlar (TPT) composite sheet, which offers mechanical strength and additional protection. Finally, while a metallic frame supports the actual module, this element is not incorporated in the present numerical modeling, because its thermal influence is considered negligible due to its small surface area [28].

In order to improve the thermal performance of PV-Ms, an innovative aluminum heat exchanger has been designed specifically for integration into PVT-Ss. The configuration comprises 49 slicks, each with its own holes, as shown in Fig. 2. 25 slicks are open to allow the heat transfer fluid to circulate in direct contact with the rear surface of the PV-M, thus maximizing heat extraction, while 24 closed layers serve as a support for a thin layer of thermal paste 0.1 mm thick, ensuring optimal and uniform heat transfer across the entire contact surface. The 24 closed slicks are hollow, meaning that the fluid circulates inside them but without direct contact with the PV-M (Fig. 2). Each slick is 19.40 mm wide and 1 mm high (Fig. 3). This dimension was determined after a detailed study showing that increasing the height of the slick leads to an increase in the temperature of the PV-M and a decrease in the energy efficiency of the fluid, as justified by studies [8,26]. At the ends of the exchanger, 30 mm high collectors at the inlet and outlet allow the fluid to be distributed evenly throughout the 49 channels, and this value of 30 mm is justified in studies [26]. Table 1 shows the dimensions of the proposed system in detail. Progressive filling from bottom to top promotes uniform circulation and limits the formation of stagnation zones,

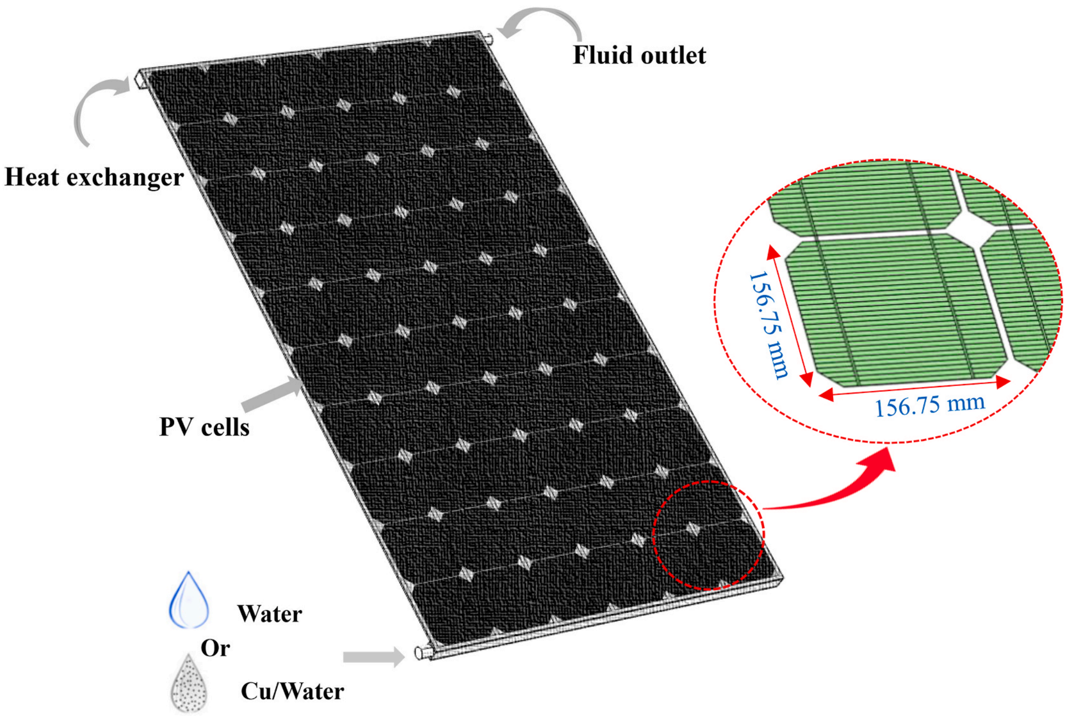

Fig. 1. Illustration of the designed PVT-S.

which improves internal convection and optimizes heat transfer to the fluid. In addition to heat transfer, the design takes mechanical constraints into account. The use of thermal paste, combined with a modular architecture, effectively minimizes the stresses caused by thermal expansion variations between the PV-M and the heat exchanger, thereby helping to enhance the reliability and durability of the system. The choice of aluminum not only ensures the lightness of the exchanger but also facilitates its manufacture, offering a robust and economical solution, as demonstrated in previous studies [26]. Overall, this configuration represents a comprehensive approach to the efficient cooling of PV-Ms integrated into PVT-Ss, combining optimized thermal performance, increased durability, and simplicity of production.

The physical and geometric description of the materials that constitute the PVT-S is summarized in detail in Table 2. This includes the various dimensions, structure, and characteristics of the components. In addition, the materials' optical criteria and the operating circumstances considered in the numerical model (such as temperatures, solar radiation, and heat transfer coefficients) are specified in Table 3.

2.2. Numerical analysis and simulation methodology

The PVT-S is analyzed employing COMSOL Multiphysics, which is based on the finite element method (FEM) software. In this work, The three-dimensional model applies the Galerkin method [33–35] to simultaneously solve the combined equations of conservation of heat, mass, and momentum. This approach ensures accurate modeling of heat and fluid transfers within the module. In order to accurately reflect the interactions between components, the model includes conjugate heat transfer, representing thermal change among fluid and PV-M. The complete simulation process, from geometry creation to result extraction, is shown in Fig. 4, which illustrates the main steps of numerical modeling.

2.2.1. Modeling assumptions and core equations

The three-dimensional model was designed to accurately capture internal temperature variations and thermal interactions inside the module. The fluid flow is considered laminar, incompressible, and stable, ensuring realistic conditions for heat transfer analysis.

Assumptions.

- ❖ Perfect thermal contact between components: the interfaces between the different PV-M or PVT-S layers are assumed to have no additional thermal resistance [26,36].
- ❖ Clean module surface: the panels are considered free of dust or dirt, ensuring that optical absorptivity remains constant and at its maximum [37,38].
- ❖ Constant thermophysical properties: materials are assumed not to change their characteristics (conductivity, heat capacity, density) with temperature [8,12,39].
- ❖ Total transparency of EVA: the EVA layer is considered completely transparent (100 % transmission), ensuring that all incident light reaches the PV cells [17,31,40].
- ❖ Heat losses limited to the front faces for PVT-Ss: only losses through the front face are considered, while the rear and side faces are treated as adiabatic, reflecting the typical insulation efficiency and reducing the model's complexity. For uncooled PV-Ms, thermal transfer at the rear is calculated as 50 % of that detected at the front, because of fewer effective cooling [41].
- ❖ Uniform ambient temperature: the surrounding air is assumed to be homogeneous, and heat losses through the module frame are neglected [26,42].

The heat produced by PV cells is mainly propagated through materials by conduction (equation (1)). In contrast, the heat exchanger ensures its transfer to the fluid through conduction and convection (equations (2)–(4)). These phenomena are represented in the numerical model, allowing overall thermal behavior of the PVT-S to be simulated accurately [26,43,44]:

$$-\left(\frac{\partial^2 T}{\partial x^2}+\frac{\partial^2 T}{\partial y^2}+\frac{\partial^2 T}{\partial z^2}\right)\left(\frac{k}{\rho.C_p}\right)=0 \tag{1}$$

$$\frac{\partial u}{\partial x}+\frac{\partial v}{\partial y}+\frac{\partial w}{\partial z}=0 \tag{2}$$

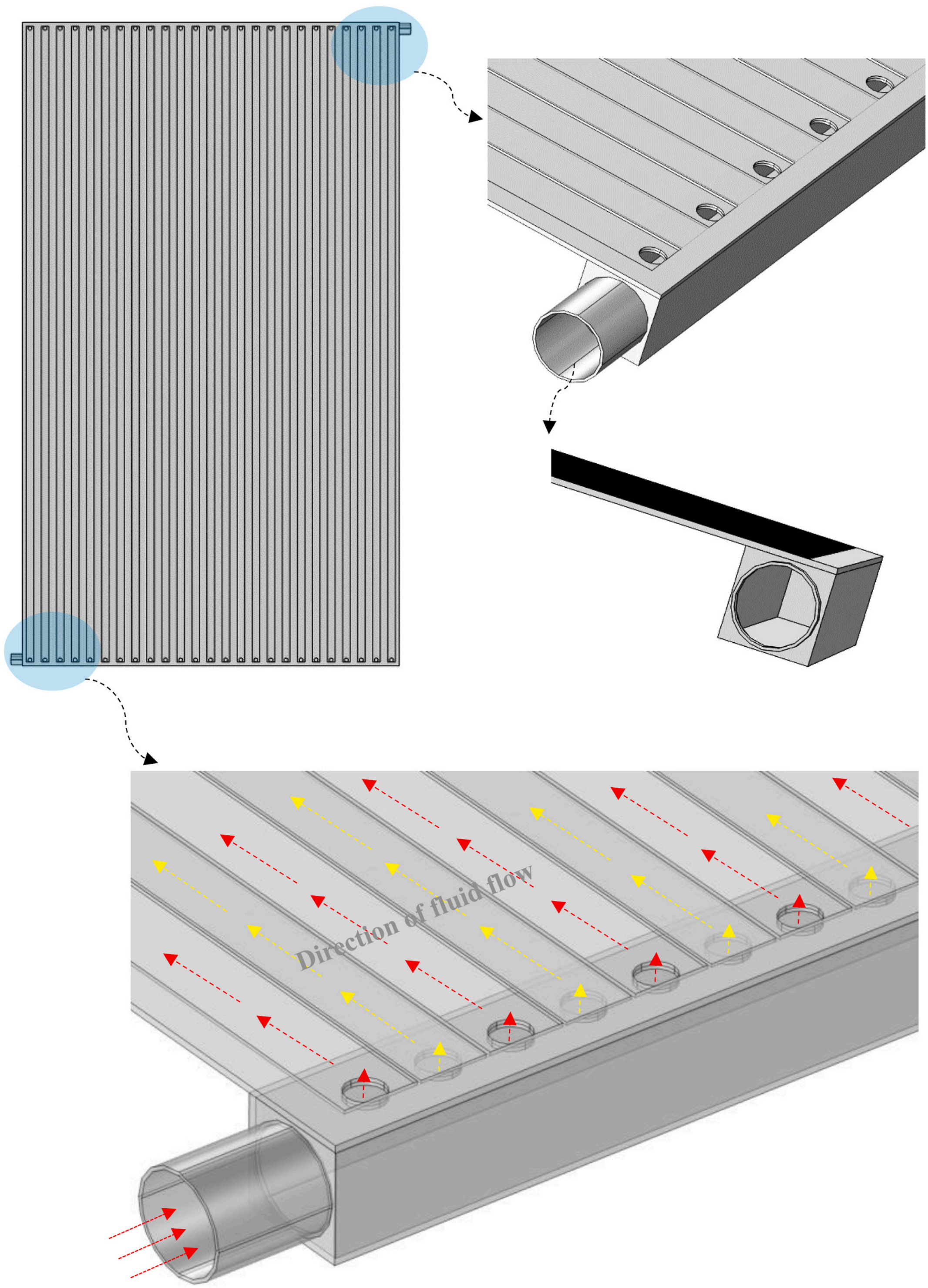

Fig. 2. Three-dimensional schematic of the novel aluminum heat exchanger with 49 microchannels (25 open, 24 closed).

$$\begin{cases} \rho_f\left(u\frac{\partial w}{\partial x}+v\frac{\partial w}{\partial y}+w\frac{\partial w}{\partial z}\right) = -\frac{\partial p}{\partial z}+\mu_f\left(\frac{\partial^2 w}{\partial x^2}+\frac{\partial^2 w}{\partial y^2}+\frac{\partial^2 w}{\partial z^2}\right) \\ \rho_f\left(u\frac{\partial v}{\partial x}+v\frac{\partial v}{\partial y}+w\frac{\partial v}{\partial z}\right) = -\frac{\partial p}{\partial y}+\mu_f\left(\frac{\partial^2 v}{\partial x^2}+\frac{\partial^2 v}{\partial y^2}+\frac{\partial^2 v}{\partial z^2}\right) \\ \rho_f\left(u\frac{\partial u}{\partial x}+v\frac{\partial u}{\partial y}+w\frac{\partial u}{\partial z}\right) = -\frac{\partial p}{\partial x}+\mu_f\left(\frac{\partial^2 u}{\partial x^2}+\frac{\partial^2 u}{\partial y^2}+\frac{\partial^2 u}{\partial z^2}\right) \end{cases} \tag{3}$$

$$(\rho_f C_{pf})\left(u\frac{\partial T_f}{\partial x}+v\frac{\partial T_f}{\partial y}+w\frac{\partial T_f}{\partial z}\right)=k_f\left(\frac{\partial^2 T_f}{\partial x^2}+\frac{\partial^2 T_f}{\partial y^2}+\frac{\partial^2 T_f}{\partial z^2}\right) \tag{4}$$

Where P corresponds to the fluid pressure, ρ is the fluid density, T is the temperature, C is the specific heat, k is the conductivity, and μ denotes its dynamic viscosity.

2.2.2. Boundary conditions

To simulate the thermal behavior of the PVT-S and PV-M correctly,

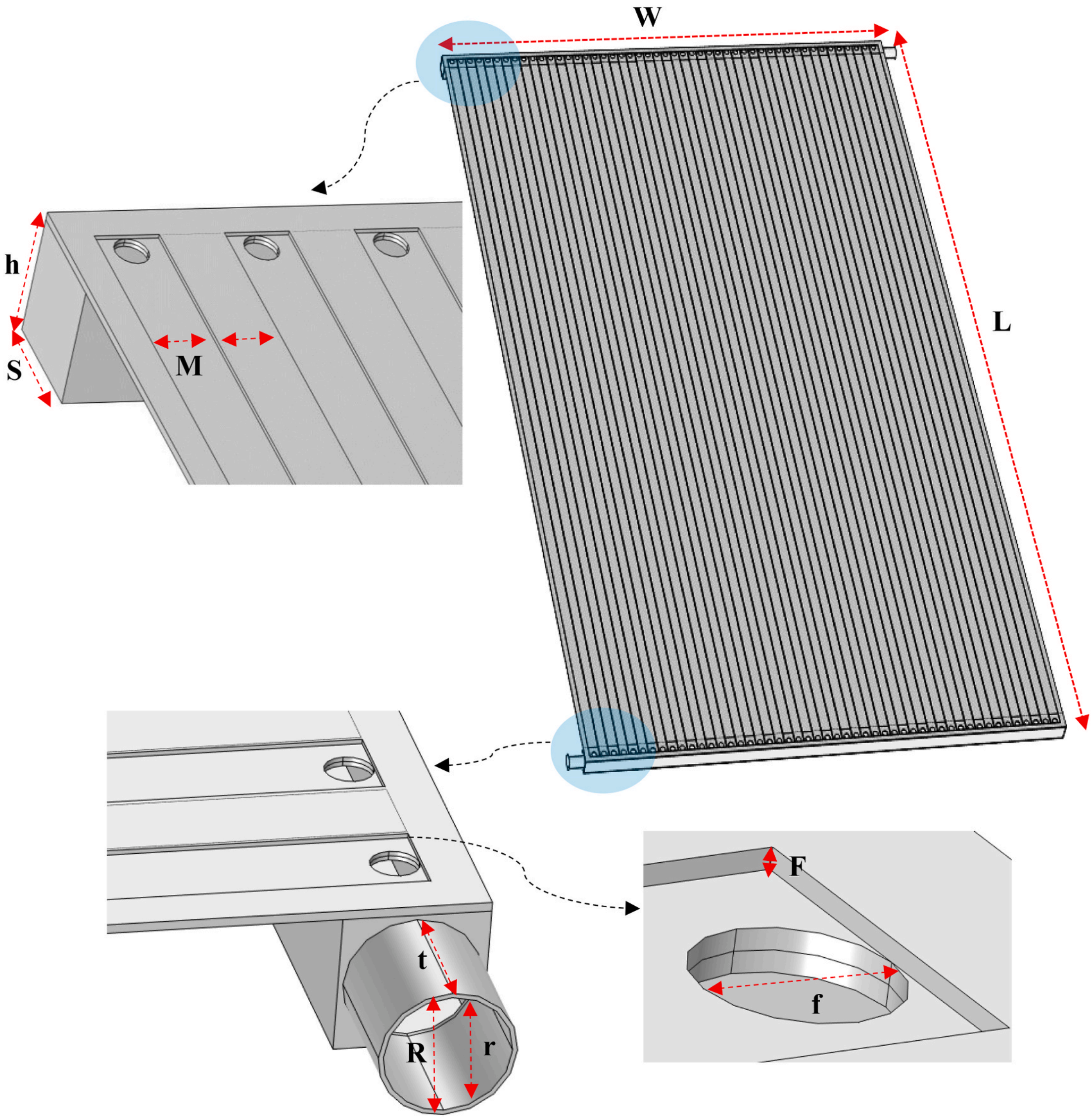

Fig. 3. Detailed presentation of the dimensions of the new 49-slick heat exchanger.

Table 1
Dimensional details of the new 49-slick heat exchanger.

Parameter	Value
Length (L)	1605.5 mm
Width (W)	970.5 mm
Fluid slick width (M)	19.40 mm
Height of the fluid collector (h)	30 mm
Width of the fluid collector (S)	30 mm
Hole diameter (f)	10 mm
Inlet collector length (t)	30 mm
Maximum inlet diameter of system (R)	14 mm
Minimum inlet diameter of the system (r)	13 mm
Height of the fluid slick (F)	1 mm

the boundary conditions (BCs) must be defined precisely. The upper surface of the module plays an important role in heat dissipation, where exchanges occur simultaneously via convection with the air and radiation (Fig. 5). For the PVT-S, the side and rear walls are considered perfectly adiabatic, preventing any additional heat exchange. Regarding fluid flow, the inlet of the exchanger is defined by an imposed temperature and MFRT, while the outlet is subject to a fixed pressure, ensuring stable and realistic circulation. A heat transfer coefficient of 150 W/m^2·K is applied to the PV-M surfaces [31,45,46], ensuring efficient transfer to the fluid. In addition, for the PVT-S, the channel walls comply with the no-slip condition, correctly simulating the interaction between the fluid and the walls. For the PV-M, heat transfer at the rear face is estimated at 50 % of that measured at the front face, due to less efficient cooling, as shown in studies [41,47,48]. All of these specifications, incorporating thermal and hydraulic aspects, are presented in Table 4 for the PVT-S and in Table 5 for the PV-M, providing an overview of the essential parameters used in the numerical simulation.

2.3. Nanofluid thermophysical properties

This study examines the impact of introducing Cu nanoparticles into pure water, which is used as a heat transfer fluid, on the new PVT-S' energy-exergy calculation. The objective is to compare the results obtained with: colling using this nanofluid, cooling with water alone and PV-M operating without cooling. In order to achieve thus purpose, several nanoparticle geometries are considered for evaluating the influence of their shape on the thermal behavior of fluid, as shown in Table 6. Additionally, the incorporation of nanoparticles significantly modifies the specific thermophysical criteria of the fluid. A volume fraction of $\varphi = 2$ % was adopted, per the literature [49]. Note that it

Table 2
Physical and geometric description of PVT-S materials [26,29,30].

Materials	Layer	Thickness (mm)	W × L (mm^2)	k [W/(m.K)]	ρ [Kg/m^3]	C_p [J/(kg.K)]
Glass	Top layer	3	970.5 x 1605.5	2200	1.8	750
Aluminum	Heat exchanger	–	970.5 x 1605.5	238	2700	900
EVA	Encapsulant	0.3	970.5 x 1605.5	0.29	935	2400
Thermal paste	Conductor	0.1	970.5 x 1605.5	1.9	2600	700
Tedlar	Bottom layer	0.3	970.5 x 1605.5	0.14	1200	1250
Silicon	Solar cell	0.19	156.75 x156.75	148	2329	703

Table 3
Optical criteria and operating conditions of PVT-S numerical model [30–32].

Symbol/Unit	Description	Values
G (W/m^2)	Intensity of incoming solar radiation	200–1200
U_t (W/m^2.K)	Heat transfer coefficient of PVT-S surface	150
T_{in} (°C)	Inlet temperature of fluid	26
ε_g	Emissivity of glass layer	0.04
P_c	PV-M's packing factor	0.95
η_{ref} (%)	Reference efficiency	14
α_c	Absorption coefficient of PV cells	0.9
τ_g	Optical transmittance of glass	0.96
$U_{g\text{-}amb}$ (W/m^2. K)	Heat transfer coefficient between glass and surrounding air	10
T_{amb} (°C)	Ambient air temperature	26
T_{ref} (°C)	Reference temperature for calculations	25
$\dot{m}$ (kg/s)	Fluid MFRT at inlet	0.0111–0.0556
B_{ref} (%/°C)	Cell's thermal efficiency coefficient	0.0045

improves heat transfer while maintaining good suspension stability. Table 7 summarizes the thermophysical characteristics of water and those of the Cu nanoparticles utilized for this modeling. The effective thermal conductivity, density, specific heat, and dynamic viscosity of the water–Cu nanofluid are estimated by equations (5)–(8) [50,51].

$$C_{Pnf} = \frac{(1-\varphi)\cdot(\rho c_p)_w + \varphi\cdot(\rho\cdot c_p)_p}{(1-\varphi)\cdot\rho_w + \varphi\cdot\rho_p} \tag{5}$$

$$\rho_{nf} = (1-\varphi)\cdot\rho_w + \varphi\cdot\rho_p \tag{6}$$

$$\mu_{nf} = \frac{\mu_w}{(1-\varphi)^{2.5}} \tag{7}$$

$$k_{nf} = \left(\frac{k_p - (m-1)\cdot\varphi\cdot(k_w - k_p) + (m-1)\cdot k_w}{k_p + (k_w - k_p)\cdot\varphi + (m-1)\cdot k_w}\right)k_w \tag{8}$$

2.4. Theoretical contextual and analysis

2.4.1. Energy assessment

To better understand the energy behavior of a PVT-S, it is useful to represent it as a single control volume, as illustrated in Fig. 6. This approach can enable detailed tracking of all incoming and outgoing energy flows. The solar energy absorbed (E_{abs}) by the PV-M is principally divided into three parts: electricity generation (E_{el}), heating of the heat transfer fluid (Q_{th}), and heat losses (Q_{loss}) via convection and radiation from exposed surfaces. Assuming a steady state, where thermal and electrical properties remain constant over time, the energy balance of this volume can be formulated as [53]:

$$E_{abs} = Q_{loss} + Q_{th} + E_{el} \tag{9}$$

The energy received by the PVT-S is quantified using equation (10), which takes into account the incident irradiance and the characteristics of the module. At the same time, heat losses to the environment, resulting from both convection with air and radiation emitted by module surfaces, are determined using equation (11) [26,43]:

$$E_{abs} = \alpha_c\cdot p_c\cdot\tau_g\cdot A_{PVT}\cdot G \tag{10}$$

$$Q_{loss} = Q_{rad} + Q_{conv} \tag{11}$$

The quantification of convective heat losses (Q_{conv}) is performed using equation (12), which takes into account the heat transfer coefficient and the temperature differences between the module surface and the ambient air. The evaluation of radiation losses (Q_{rad}) is performed using equation (13), considering the radiative properties of the module

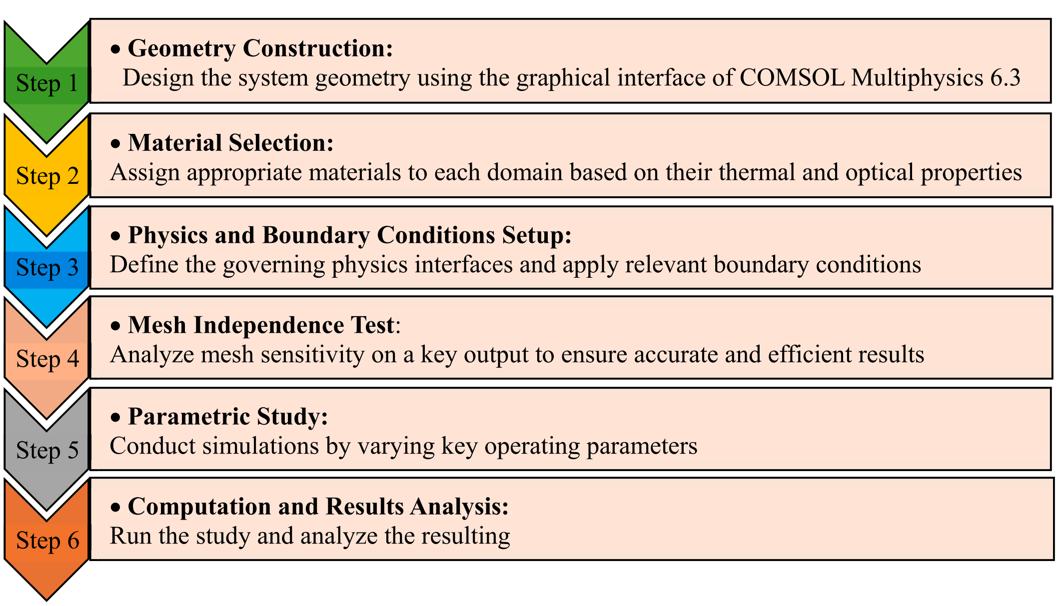

Fig. 4. Overall flow of the digital process for thermal and electrical analysis of PVT-S.

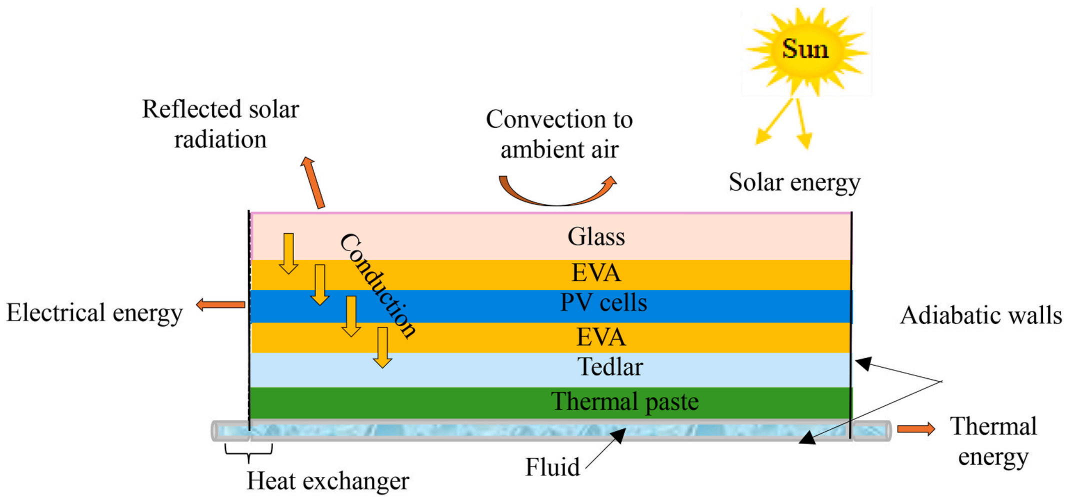

Fig. 5. Distribution of PVT-S BCs.

Table 4
PVT-S border setup.

Position	Boundary definitions
System outlet, controlled by pressure **BC**	$P_{out} = 0$
Top boundary subjected to convective heat transfer	$-n \cdot q = h_{g-amb} \cdot (T_{amb} - T_g)$
System inlet, defined by imposed temperature and **MFRT**	$T = T_{in}, \dot{m} = \dot{m}_{in}$
Upper boundary surface with applied inward heat flux	$-k_g \frac{\partial T_g}{\partial z} = G$
No-slip at solid–fluid contact areas	$u = v = w = 0$
Upper surface exposed to radiative heat losses	$-n \cdot q = \varepsilon_g \cdot \sigma \cdot ({T_{sky}}^4 - {T_g}^4)$
Junction region between the heat exchanger and the fluid domain	$\left(\frac{\partial T}{\partial n}\right)_{fluid} = \frac{k_{solid}}{k_{fluid}} \left(\frac{\partial T}{\partial n}\right)_{solid}$
Thermal insulation at all other surfaces	$\frac{\partial T}{\partial n} = 0$

Table 5
PV-M border setup.

Position	Boundary definitions
The upper and lower surfaces are subject to heat transfer by convection	$-n \cdot q = h_{g-amb} \cdot (T_{amb} - T_g)$
Upper boundary surface with applied inward heat flux	$-k_g \frac{\partial T_g}{\partial z} = G$
Upper surface exposed to radiative heat losses	$-n \cdot q = \varepsilon_g \cdot \sigma \cdot ({T_{sky}}^4 - {T_g}^4)$

and the energy exchange with the environment [43,54]:

$$Q_{conv} = A_{PVT} \cdot \left(T_g - T_{amb}\right) \cdot h \text{ where } h = 5.7 + 3.8 \cdot V \tag{12}$$

$$Q_{rad} = \left({T_g}^4 - {T_{sky}}^4\right) \cdot A_{PVT} \cdot \varepsilon_g \cdot \sigma \tag{13}$$

In this equation, σ represents the Stefan-Boltzmann constant, A_{PVT} is the surface area of the PVT-S, and the sky temperature (T_{sky}) is calculated from the ambient temperature using the equation below [53]:

$$T_{sky} = 0.0552 \bullet T_{amb}{}^{1.5} \tag{14}$$

The electrical power (E_{el}) of the system is calculated using the following equation [8,43,54]:

$$E_{el} = p_c \cdot \tau_g \cdot \alpha_c \cdot G \cdot A_{PVT} \cdot \eta_{ref} \cdot \left(1 - \beta_{ref} \cdot \left(T_c - T_{ref}\right)\right) \tag{15}$$

The temperature of the cells (T_c) is calculated using the following equation [8,43,54]:

$$T_c = \frac{P_c \cdot G \cdot \left(\tau_g \cdot \alpha_c - \eta_{ref}\right) + \left(U_{g-amb} \cdot T_{amb} + U_t \cdot T_{ted}\right)}{\left(U_{g-amb} + U_t\right)} \tag{16}$$

The EEF (η_{el}) is calculated using the following equation [8,43,54]:

$$\eta_{el} = \eta_{ref} \cdot \left(1 - \beta_{ref} \cdot \left(T_c - T_{ref}\right)\right) \tag{17}$$

The heat recovered (Q_{th}) by the fluid is calculated as [31,55]:

$$Q_{th} = \dot{m} \cdot C_f \cdot \left(T_{out} - T_{in}\right) \tag{18}$$

Table 6
Geometric configuration of nanoparticles and shape factor (m) [52].

Shapes	Particle form	Shape factor (m)
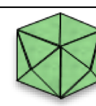	Octahedron	1.18
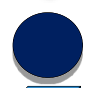	Sphere	3.0
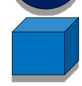	Bricks	3.70
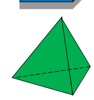	Tetrahedron	4.06
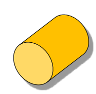	Cylinder	4.90
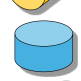	Platelet	5.70
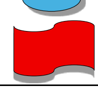	Blade	8.90

Table 7
Thermophysical data for water and Cu nanoparticles [51,52].

Materials	k (W/(m.K))	C_p (J/(kg.K)	ρ (kg/m^3)	μ (Pa·s)
Water	0.6	4181.8	998.2	0.001003
Cu	401	385	8933	–

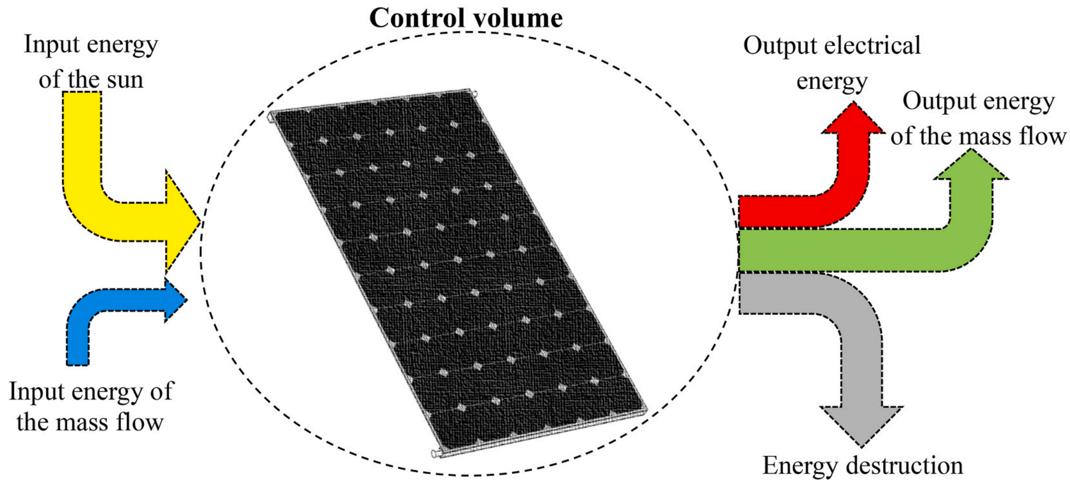

Fig. 6. Energy balance of a PVT-S treated as a control volume.

The TEF (η_{th}) is calculated using the following equation [31,55]:

$$\eta_{th} = \frac{Q_{th}}{E_{abs}} \tag{19}$$

The overall system efficiency (η_{ov}) is calculated using the following equation [31,55]:

$$\eta_{ov} = \frac{Q_{th}}{E_{abs}} + \frac{E_{el}}{E_{abs}} \tag{20}$$

2.4.2. Exergy assessment

Energy analysis is limited to quantifying the total quantity of energy, while exergy analysis, also included in this work, evaluates the quality of energy relative to that provided by the sun. This approach takes into account irreversibility, entropy losses, and uneven temperature distribution within the system. Exergy is analyzed in a similar way to energy, but it provides additional information on the actual efficiency of the system. Additionally, the exergy flow diagram of the PVT-S is shown in Fig. 7. When the system is treated as a single control volume operating under steady-state conditions, the exergy can be expressed by the following equation [56]:

$$\dot{X}_{sun} = \dot{X}_{el} + \dot{X}_{des} + \dot{X}_{th} \tag{21}$$

where $\dot{X}_{sun}$, $\dot{X}_{th}$, $\dot{X}_{el}$, and $\dot{X}_{des}$ represent the input exergy, the thermal exergy, the electrical exergy, and the destroyed exergy (losses), respectively.

The exergy input ($\dot{X}_{sun}$) and the output exergy rate ($\dot{X}_{out}$) are expressed by the following equation [57]:

$$\dot{X}_{sun} = E_{abs} \cdot \left[1 + \frac{1}{3}\left(\frac{T_{amb}}{T_{sun}}\right)^4 - \frac{4}{3}\left(\frac{T_{amb}}{T_{sun}}\right)\right] \tag{22}$$

Where T_{sun} denotes the Sun's blackbody surface temperature, taken as 5770 K [57].

$$\dot{X}_{out} = \dot{X}_{el} + \dot{X}_{th} \tag{23}$$

The thermal exergy ($\dot{X}_{th}$) and electrical exergy ($\dot{X}_{el}$) can be determined according to the following relations [58]:

$$\dot{X}_{th} = \dot{m} \cdot c_p \cdot (T_{out} - T_{in}) \cdot \left(1 - \frac{T_{amb}}{T_{out}}\right) \tag{24}$$

$$\dot{X}_{el} = \eta_{el} \cdot E_{abs} \cdot \left[1 + \frac{1}{3}\left(\frac{T_{amb}}{T_{sun}}\right)^4 - \frac{4}{3}\left(\frac{T_{amb}}{T_{sun}}\right)\right] \tag{25}$$

The evaluation of electrical exergy (ε_{el}), thermal exergy (ε_{th}), and the overall exergy (ε_{PVT}) efficiency is carried out through the following relations [58]:

$$\varepsilon_{th} = \frac{\dot{X}_{th}}{\dot{X}_{sun}} \tag{26}$$

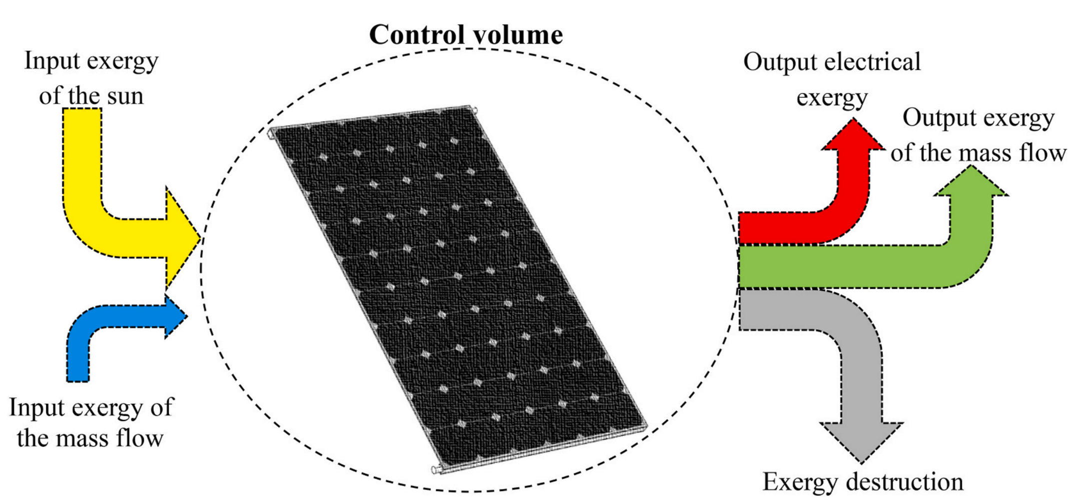

Fig. 7. Representation of exergy transfers and losses in the PVT-S.

$$\varepsilon_{el} = \frac{\dot{X}_{el}}{\dot{X}_{sun}} \tag{27}$$

$$\varepsilon_{PVT} = \frac{\dot{X}_{out}}{\dot{X}_{sun}} = \varepsilon_{el} + \varepsilon_{th} = 1 - \frac{\dot{X}_{loss}}{\dot{X}_{sun}} = \frac{\dot{X}_{el} + \dot{X}_{th}}{\dot{X}_{sun}} \tag{28}$$

2.4.3. Exergy destruction and entropy generation assessment

Due to heat transfer and hydrodynamic friction losses within the flow channels, part of the available exergy is destroyed. These irreversible processes decrease the ability of the system to effectively convert solar energy into useful thermal and electrical outputs. The resulting exergy destruction (also known as exergy loss) highlights the influence of internal dissipation and non-ideal temperature gradients on the overall performance of the PVT-S. The evaluation of this parameter, which is very important for assessing the quality of the converted energy, is carried out utilizing equation (29) as follows [59]:

$$\dot{X}_{des} = \dot{X}_{sun} - \dot{X}_{el} - \dot{X}_{th} \tag{29}$$

Another key parameter in the thermodynamic assessment of the PVT-S is the entropy generation, which indicates the irreversibilities caused by heat transfer and fluid friction. It measures the loss of available energy and helps evaluate the system's real efficiency. The entropy generation is computed by equation (30) as follows [60]:

$$\dot{S}_{gen} = \frac{\dot{X}_{des}}{T_{amb}} \tag{30}$$

2.4.4. Sustainability assessment

Here, the sustainability of a system is measured by its ability to convert available energy while reducing environmental impacts efficiently. In order to quantify this performance, the sustainability index (SI) combines exergy efficiency to reflect the actual value and quality of the energy produced. Note that maximizing this index enhances overall energy efficiency and limits losses and environmental impacts. Thus, the sustainability index is determined employing the following formula [61, 62]:

$$SI = \frac{1}{1 - \varepsilon_{PVT}} \tag{31}$$

2.4.5. Annual energy production assessment

The economic viability of PV-Ms and PVT-Ss is analyzed by assessing their capacity to produce energy over their entire lifespan. To do this, annual production is determined utilizing equations (32)–(34), which incorporate the solar yearly irradiance (G_t) measured in El Jadida (Morocco) and the annual degradation rate (dg) of PV-Ms, estimated at 0.8 % by the manufacturer. These calculations provide a solid basis for energy estimation and exergy analysis, allowing the efficiency and quality of the energy produced by the system to be examined [63].

$$E_{ele} = \left(365 \cdot G_t \cdot \eta_{el} \cdot A_{pv}\right) \cdot (1 - dg)t^{-1} \tag{32}$$

$$E_{th} = (365 \cdot G_t \cdot \eta_{th} \cdot A_{th}) \cdot (1 - dg)t^{-1} \tag{33}$$

$$E_{ntotal} = E_{th} + E_{ele} \tag{34}$$

2.5. Meshing procedure and grid independence verification

A mesh independence analysis is performed in order to guarantee the reliability of the numerical results of the PVT-S using COMSOL Multiphysics® [64]. This allows for optimal adaptation to the physical constraints imposed by the model. To assess the impact of mesh resolution on the precision of numerical results, several configurations were tested. The comparison is based primarily on two essential parameters of system operation, namely the temperature reached by the PV cells and the maximum fluid pressure, as well as the calculation time associated with each configuration. The analysis was carried out under representative conditions, with a MFRT set at 0.0556 kg/s and solar irradiance of 1000 W/m^2 to ensure consistency of results between the different meshes. The simulations show that varying the mesh size does not result in any significant change in either the temperature of the PV cells or the maximum pressure of the system. As Table 8 shows, the differences between the meshes of 29, 651, 575 elements and 49, 733, 846 elements remain very small. Based on these observations, the mesh of 29, 651, 575 elements is selected for the final numerical analysis (Fig. 8), as it offers satisfactory accuracy while reducing calculation time. The relative errors observed for the PV cell temperature and maximum pressure remain limited to 0.005 % and 0.08 %, confirming the reliability of this mesh configuration.

2.6. Numerical code authentication

The PVT-S model was validated using a combination of numerical and experimental approaches, as shown in Fig. 9. First, our numerical results were compared with those of Attia et al. [65], who studied the optimization of a PVT-S measuring 1200 mm by 540 mm with a power of 90 W and a zigzag channel. The temperature of the PV cells was chosen as the main criterion and evaluated for a range of irradiances from 200 to 1000 W/m^2, with a MFRT of 0.003 kg/s and an ambient and inlet temperature of 27 °C. The comparisons shown in Fig. 9a show a close match, confirming that the model accurately reproduces the system's thermal behavior under different solar conditions. At the same time, experimental validation was carried out based on the work of Azeez et al. [63], who studied a new solar water collector measuring 360 mm × 670 mm and rated at 30 W under conditions of high cooling demand. EEF was chosen as the performance indicator and evaluated for several MFRTs, ranging from 0.01 to 0.07 kg/s, under 800 W/m^2 radiation. The results shown in Fig. 9b reveal a strong agreement between the simulated data and the experimental measurements, reinforcing the credibility of the model and its ability to reflect the system's actual behavior. The maximal deviations observed are small, with a maximum of 4.80 % and 1.15 % for numerical and experimental validations, respectively. The differences can be attributed to modeling assumptions, geometric simplifications, or variations in the materials' thermophysical criteria. However, the results' overall alignment indicates that our model is sufficiently robust to capture the essential thermal phenomena and can be used confidently for predictive analyses and future optimizations of the PVT-S.

3. Results and discussion

This study focuses on a new PVT-S, whose performance has been analyzed in terms of various aspects: energy, sustainability, exergy, annual production, as well as exergy destruction and entropy generation. Two types of cooling fluids, namely water alone and a Cu/water nanofluid, were examined to compare their efficiency. In addition, different forms of Cu nanoparticles were evaluated to identify the one offering the best performance. The analyses were conducted based on radiation (200–1200 W/m^2), and MFRTs (0.0111–0.0556 kg/s).

3.1. PV module alone

Fig. 10 highlights the temperature distribution inside PV-Ms. We can see that the hottest point is in the center. This thermal concentration results from the density of solar cells in this area, which convert solar radiation into electricity while producing heat. In contrast, the edges of the modules have lower temperatures. This can be attributed to more efficient heat dissipation to the outside, while the center experiences greater thermal confinement.

Fig. 11 displays the influence of solar irradiance on the temperature of PV cells, electrical power, and EEF. The results clearly show a gradual increase in cell temperature, from 33.899 °C to 69.148 °C, alongside an

Table 8
Comparison of mesh sizes in terms of PV cell temperature, maximum pressure, and calculation time.

Mesh type	Number of elements	Computation time (s)	T_c (°C)	Relative error (%)	ΔP (Pa)	Relative error (%)
Coarser	2,472,867	4251	34,345	–	250.13	–
Coarse	4,415,133	7242	34,35	0.042	256.86	2.690
Normal	11,403,390	10,852	34,354	0.031	261.74	1.899
Fine	29,651,575	13,572	34,356	0.015	264.93	1.218
Finer	49,733,846	17,316	34,357	0.005	265.16	0.08

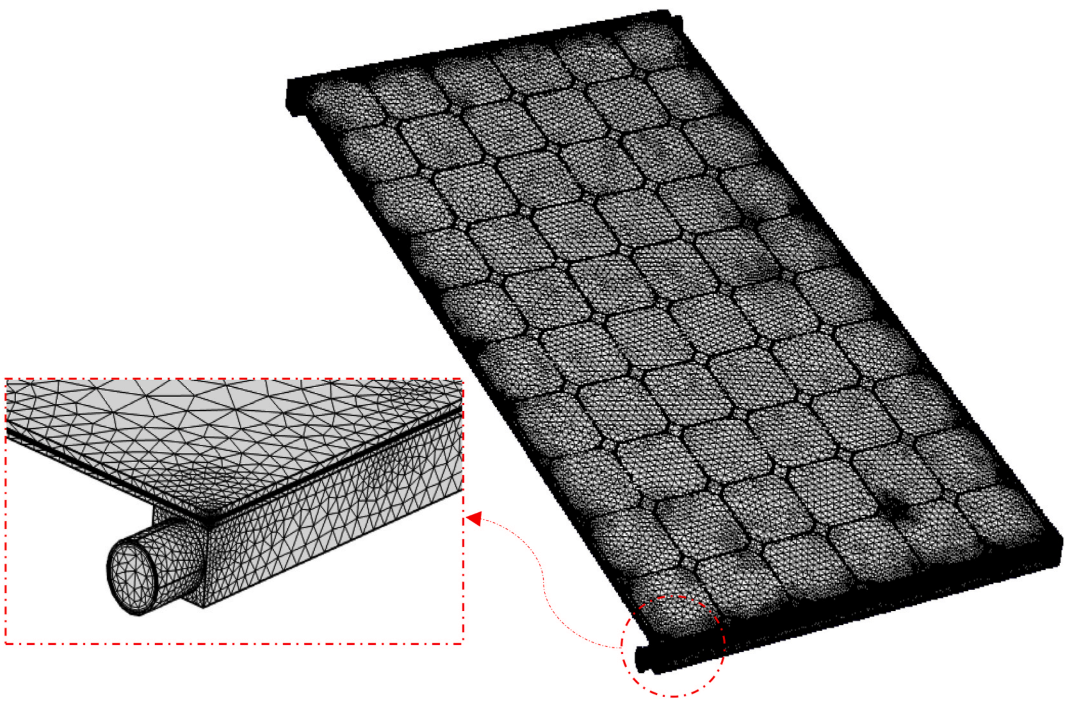

Fig. 8. Overview of the mesh structure applied to the PVT-S.

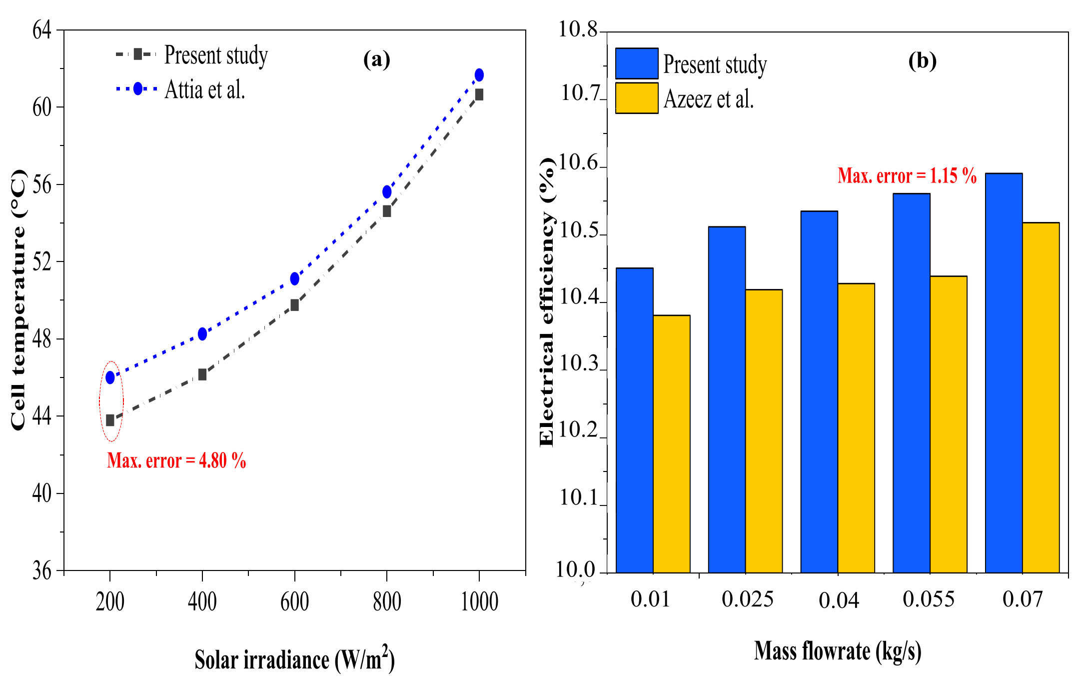

Fig. 9. Validation of the PVT-S model through numerical and experimental comparisons.

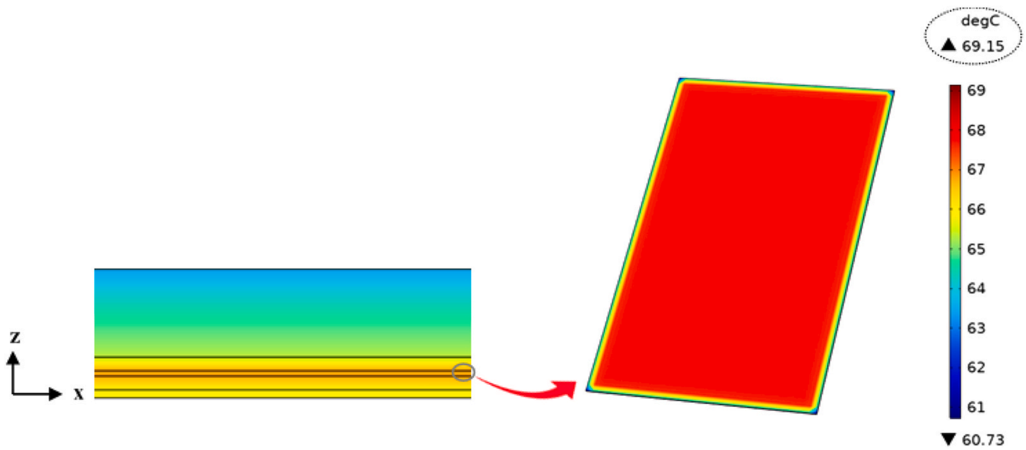

Fig. 10. Temperature distribution of the uncooled PV-M under 1000 W/m^2, showing a peak temperature at the center.

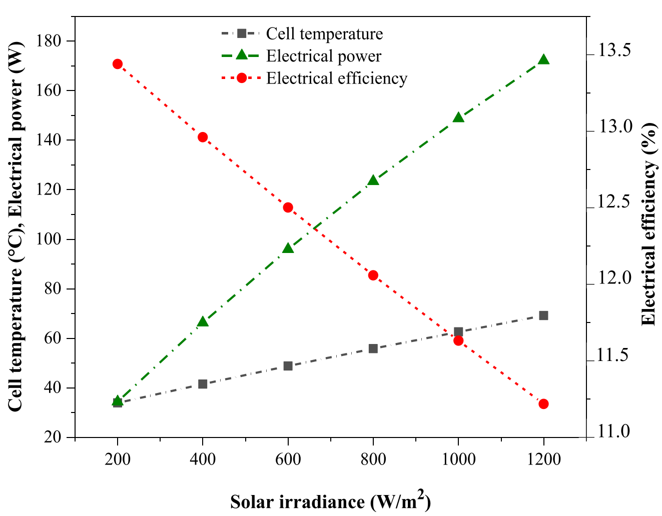

Fig. 11. Variation of PV cell temperature, electrical power, and EEF with solar irradiance (200–1200 W/m^2) for an uncooled PV-M.

increase in electrical power generated, from 34.374 W to 172.163 W, when irradiance increases from 200 to 1200 W/m^2. This change reflects the dual effects of the increased incident radiative flux: (1) enhanced PV-M conversion, and (2) increased heat accumulation in the cells. However, this rise in temperature negatively impacts EEF, which decreases significantly from 13.439 % to 11.218 %. This behavior can be explained by the internal resistance increment and in open-circuit voltage reduction as cells temperature rises, per thermosensitive mechanisms intrinsic to semiconductor materials.

3.2. Influence of nanoparticle shape

Fig. 12 displays the effect of the morphology of Cu nanoparticles on PVT-S performance. Seven different shapes (i.e., Octahedron, Sphere, Bricks, Tetrahedron, Cylinder, Platelet, and Blade) are examined. The results clearly show that particle geometry influences both the temperature distribution of the PV cells and the energy and electrical yields of the system. The cells reach the highest temperature of 34.381 °C with octahedral nanoparticles, whereas the lowest temperature of 34.356 °C is achieved with Blade particles, as shown in Fig. 12a. Note that this behavior suggests that local heat dissipation is modulated by particle geometry, which affects the thermal gradient and heat transfer efficiency. Additionally, Analysis of the heat transfer fluid's performance shows that the use of Cu/water nanofluid significantly improves the

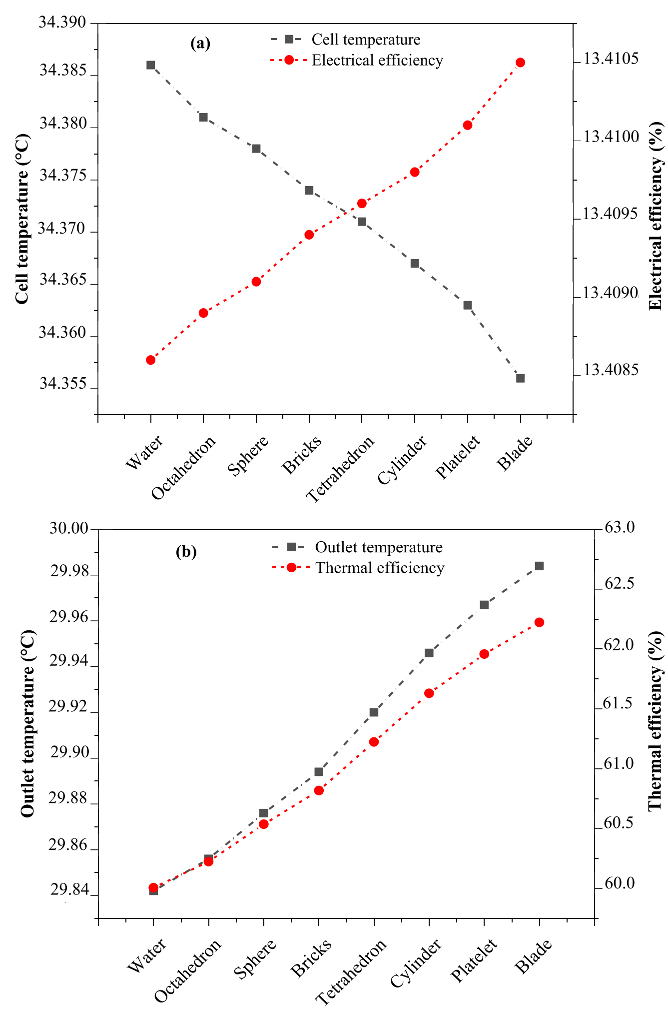

Fig. 12. Impact of Cu nanoparticle morphology on (a) PV cell temperature and EEF, and (b) fluid outlet temperature and TEF, at G = 1000 W/m^2.

outlet temperature compared to water alone, as shown in Fig. 12b, highlighting the effectiveness of nanofluids for heat extraction. Among all the shapes studied, Blade-type nanoparticles stand out for their overall best performance, reaching a maximum outlet temperature of 29.984 °C, an EEF of 13.41 %, and a TEF of 62.22 %. This superiority is directly related to their high form factor (m = 8.9). A higher form factor increases the effective thermal conductivity of the nanofluid, as shown in equation (8), and promotes more efficient heat transfer by enhancing the interactions between the fluid and the particles. Thus, the shape of the nanoparticles directly influences the heat transfer mechanism since Blade particles, due to their geometry, increase the contact surface with the fluid and improve local convection, which reduces the overall thermal resistance and optimizes heat extraction from PV cells. These results clearly show that choosing the appropriate nanoparticle geometry plays a strategic role in improving both the electrical and thermal performance of PVT-S, offering an effective path for optimizing hybrid solar systems.

3.3. Solar radiation impact

In this section, the evaluation focuses on the thermo-energetic response of an innovative PVT-S subjected to a solar irradiance range between 200 and 1200 W/m^2. Two heat transfer fluids are considered in this work, i.e., pure water and Cu/water nanofluid and the latter using blade-shaped nanoparticles due to their proven superiority in terms of performance compared to other geometries. The MFRT is kept constant at 0.0556 kg/s to ensure uniform comparison conditions. The analysis covers both the PV-M temperature evolution, outlet fluid, energy-exergy calculation, and thus providing an integrated view of the system's overall efficiency.

Fig. 13a shows that the cell temperature increases with irradiance while the EEF decreases, and this trend can be explained by well-known physical mechanisms in PV-Ms. As solar irradiance increases from 200 to 1200 W/m^2, the amount of radiative flux absorbed by the module increases, leading to a gradual accumulation of heat and a rise in cell temperature, from 27.666 to 36.071 °C for water and from 27.618 to 36.016 °C for Cu/water nanofluid. This increase in temperature directly affects electrical performance, as the rise in temperature reduces open-circuit voltage and maximum power, in line with the thermal sensitivity of semiconductor materials. As a result, the EEF gradually decreases with irradiance, from 13.832 % to 13.302 % for water and from 13.835 % to 13.305 % for the Cu/water nanofluid, illustrating the direct link between the rise in cell temperature and the decrease in their EEF.

Fig. 13b shows that the Cu/water nanofluid keeps the cells at a temperature slightly lower than that of water alone, with a maximum difference of approximately 0.055 °C, resulting in a marginal but noticeable gain in EEF of approximately 0.003 %. This trend results from the improved thermal properties of the nanofluid, which increases thermal conductivity and promotes better heat transfer from the rear surface of the cells to the fluid. By limiting heat accumulation in the cells, the nanofluid reduces the impact of temperature on open-circuit voltage and maximum power, thus maintaining slightly higher electrical performance. Although these differences appear small in absolute terms, they physically reflect the nanofluid's effectiveness in managing heat, avoiding hot spots, and ensuring more uniform heat distribution. This confirms the value of nanofluids in optimizing the cooling of PV-Ms integrated into PVT-Ss, particularly in high-irradiance conditions where heat dissipation becomes a key factor in maintaining module efficiency and durability.

Fig. 14 shows the effect of solar irradiance on the fluid outlet temperature and TEF of the PVT-S for water and Cu/water nanofluid. It can be seen that the outlet temperature increases with irradiance, rising from 26.685 °C to 30.845 °C for water and from 26.709 °C to 30.995 °C for Cu/water nanofluid when irradiance varies from 200 to 1200 W/m^2. This increase reflects the increased absorbed radiative flux and the thermal conversion efficiency of the system. At the same time, TEF increases with irradiance, from 53.493 % to 63.059 % for water and from 55.367 % to 65.011 % for the nanofluid. The relative difference between the two fluids reaches approximately 1.87 % at low irradiance and 1.95 % at high irradiance, showing that Cu/water nanofluid systematically improves heat transfer compared to water alone. This improvement is due to the higher thermal conductivity of the nanofluid and the

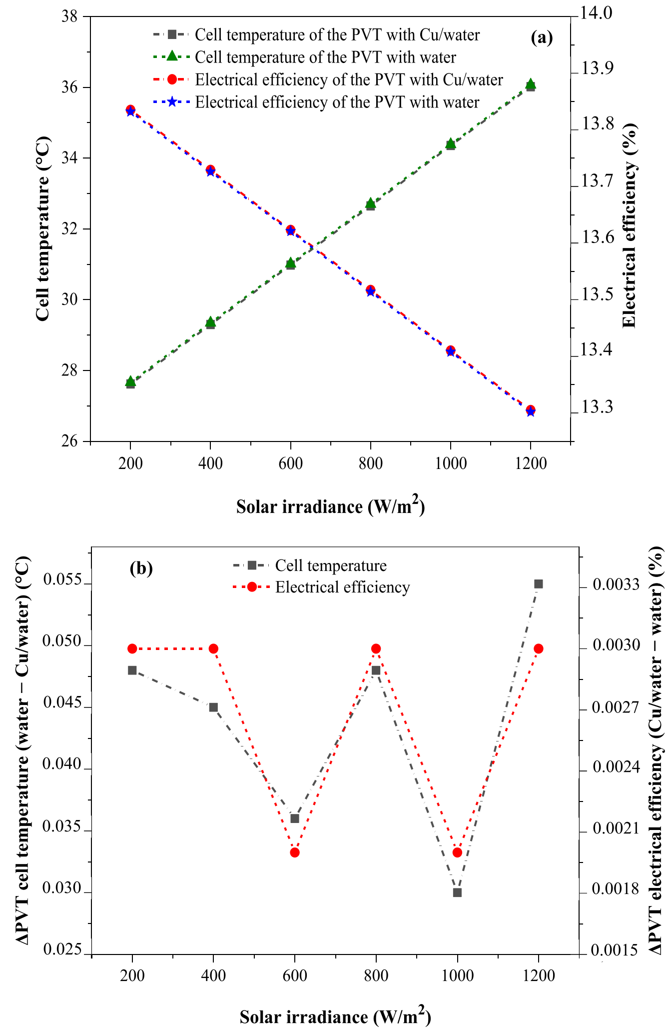

Fig. 13. Impact of heat-transfer fluid type (water and Cu/water nanofluid) and solar irradiance (200–1000 W/m^2) on (a) PV cell temperature and EEF, and (b) the difference in PV cell temperature and EEF between the two fluids.

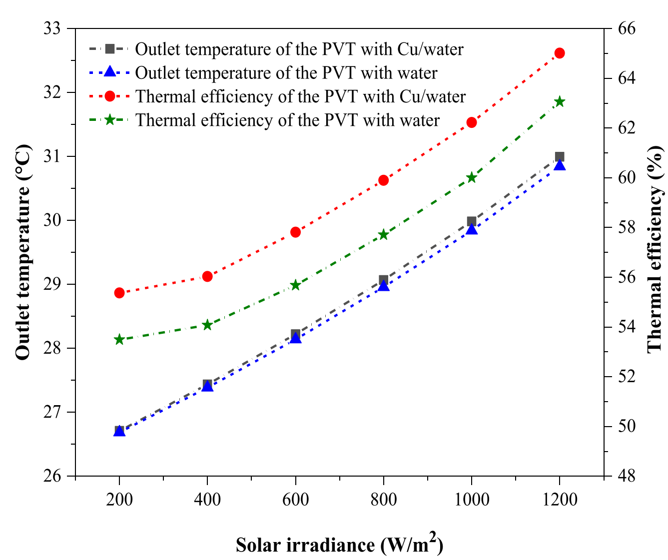

Fig. 14. Impact of heat-transfer fluid type (water and Cu/water nanofluid) and solar irradiance (200–1000 W/m^2) on outlet fluid temperature and TEF.

increased particle-fluid interaction, which promotes more efficient heat extraction generated by the PV cells. These results demonstrate that the use of Cu/water nanofluid maintains higher outlet temperatures and optimizes overall TEF, confirming the importance of fluid selection for the performance of PVT-Ss under high irradiance.

Exergy analysis provides an essential complement to energy assessment, as it allows for evaluating not only the quantity but also the quality of the converted energy. As shown in Fig. 15, solar irradiance significantly influences thermal and overall exergy efficiencies using water or Cu/water nanofluid. As expected, the results indicate that the electrical exergy efficiency is undistinguishable to EEF. However, the thermal exergy efficiency increases with irradiance, rising from 0.131 % to 1.079 % for water and from 0.140 % to 1.146 % for Cu/water when irradiance enhances (200–1200 W/m^2). The contribution of the nanofluid results in a relative gain of approximately 6 % at high irradiance, confirming the positive effect of nanoparticles on heat transfer. For its part, the overall exergy efficiency changes from 13.963 % to 14.381 % with water and from 13.975 % to 14.451 % with Cu/water, representing a relative improvement of close to 0.5 % in favor of the nanofluid. Although modest, this gain remains significant in optimizing total efficiency, especially in environments subject to high levels of irradiance.

3.4. Mass flow rate impact

This section evaluates the thermo-energetic response of an innovative PVT-S subjected to MFRTs ranging from 0.0111 to 0.0556 kg/s, considering pure water and a Cu/water nanofluid with Blade nanoparticles, under a constant irradiance of 1000 W/m^2. The analysis focuses on the thermal evolution of the module and the outlet fluid, as well as on energy-exergy evaluation.

Fig. 16 illustrates the MFRT impact of the Cu/water nanofluid on the PC cells temperature. Increasing the MFRT significantly improves cooling by enhancing convective transfer, decreasing the average cell temperature, and producing a more uniform thermal distribution. The reduced fluid velocity results in limited heat exchange when the MFRT is low (0.0111 kg/s). The fluid temperature gradually increases along the channel, which causes effective cooling at the inlet but then leads to a temperature rise in the upper part of the system, generating an inhomogeneous distribution and the potential formation of hot spots. Conversely, at higher MFRT (0.0556 kg/s), the fluid velocity reduces the thermal boundary layer thickness, promotes a higher convection coefficient, and maintains a more uniform fluid temperature throughout the flow, which homogenizes the temperature of the cells and reduces thermal gradients. Cu/water nanofluid amplifies this effect due to its improved thermal conductivity. These results confirm that mass flow control is a key parameter for simultaneously optimizing EEF by limiting cell heating and PVT-S durability and reducing local thermal stresses.

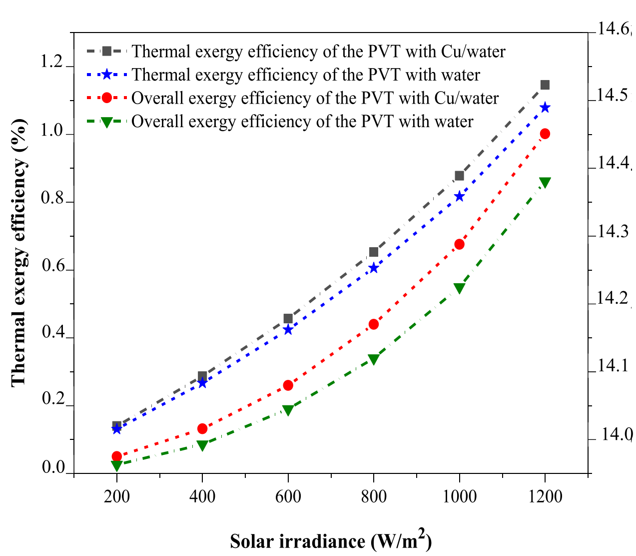

Fig. 15. Variation of thermal exergy and overall exergy efficiency of the PVT-S with solar irradiance (200–1000 W/m^2) for the two heat-transfer fluids (water and Cu/water nanofluid).

Fig. 17a highlights the effect of MFRT on the PV cells temperature and PVT-S EEF cooled by clear water and nanofluid, respectively. For both fluids, increasing the MFRT improves cooling, resulting in a significant decrease in cell temperature. In fact, the temperature drops from 44.084 °C to 34.386 °C with water, a reduction of nearly 22 %, and from 43.978 °C to 34.356 °C with Cu/water nanofluid, corresponding to a decrease of approximately 21.9 % for escalating MFRT (0.0111–0.0556 kg/s). The slight advantage observed with the nanofluid can be explained by the thermal conductivity and heat transfer criteria enhancement using Cu nanoparticles. At the same time, EEF follows the opposite trend, increasing with higher MFRTs due to the reduction in cell temperature, which limits recombination losses and maintains a higher open-circuit voltage. Thus, for water, efficiency rises from 12.797 % to 13.408 %, while for Cu/water nanofluid, it increases from 12.804 % to 13.410 %. The difference remains small but constant and confirms that the nanofluid maintains a slightly higher efficiency thanks to more efficient thermal management. The differences in cell temperature and EEF between water and Cu/water nanofluid are shown in detail in Fig. 17b.

These results confirm that the strategy of increasing MFRT to augment the PVT-S cooling and EEF simultaneously is innovative. Although the addition of Cu nanoparticles produces only modest differences, it is an interesting optimization lever, especially in prolonged operating conditions where temperature control is critical for durability and performance stability.

The evolution of the fluid outlet temperature and TEF as a function of MFRT is shown in Fig. 18 for PVT-Ss cooled by water and Cu/water nanofluid. It can be seen that for both fluids, the outlet temperature decreases (40.785–29.842 °C) and (41.452–29.984 °C) using water and nanofluid, respectively with rising MFRT (0.0111–0.0556 kg/s). This decrease can be explained by the reduction in the fluid's residence time in the module and by the increase in convective transfer, which allows the fluid to extract heat more efficiently. The Cu/water nanofluid shows a slightly higher temperature at low MFRTs due to its higher thermal conductivity. TEF increases with MFRT, rising from 46.183 % to 60.006 % for water and from 48.267 % to 62.223 % for nanofluid. This improvement can be explained by the fact that when the fluid flows faster, the temperature difference between the fluid and the module remains higher over a larger surface area, promoting more efficient heat transfer and limiting losses due to cell overheating. These results demonstrate that increasing the MFRT is an effective way to optimize thermal performance and that the use of Cu/water nanofluid offers additional benefits thanks to its improved conductivity and fluid-module interaction.

The increase in MFRT directly influences the thermal and overall exergy efficiency of the PVT-S, as shown in Fig. 19. For both fluids, a decrease in exergy efficiency is observed when the MFRT increases from 0.0111 to 0.0556 kg/s. The thermal exergy efficiency drops from 2.336 % to 0.817 % for water and from 2.546 % to 0.878 % for Cu/water nanofluid, while the overall exergy efficiency decreases from 15.133 % to 14.225 % for water and from 15.350 % to 14.288 % for the nanofluid. The fluid's residence time in the module reduces at high MFRTs, which limits heat accumulation and devalues temperature deviation between fluid and PV-M surface, thus decreasing the recoverable exergy.

3.5. Entropy generation and exergy destruction analysis

Exergy destruction and entropy generation are essential indicators for assessing irreversible losses in energy systems. Exergy destruction represents the amount of useful energy lost due to thermodynamic

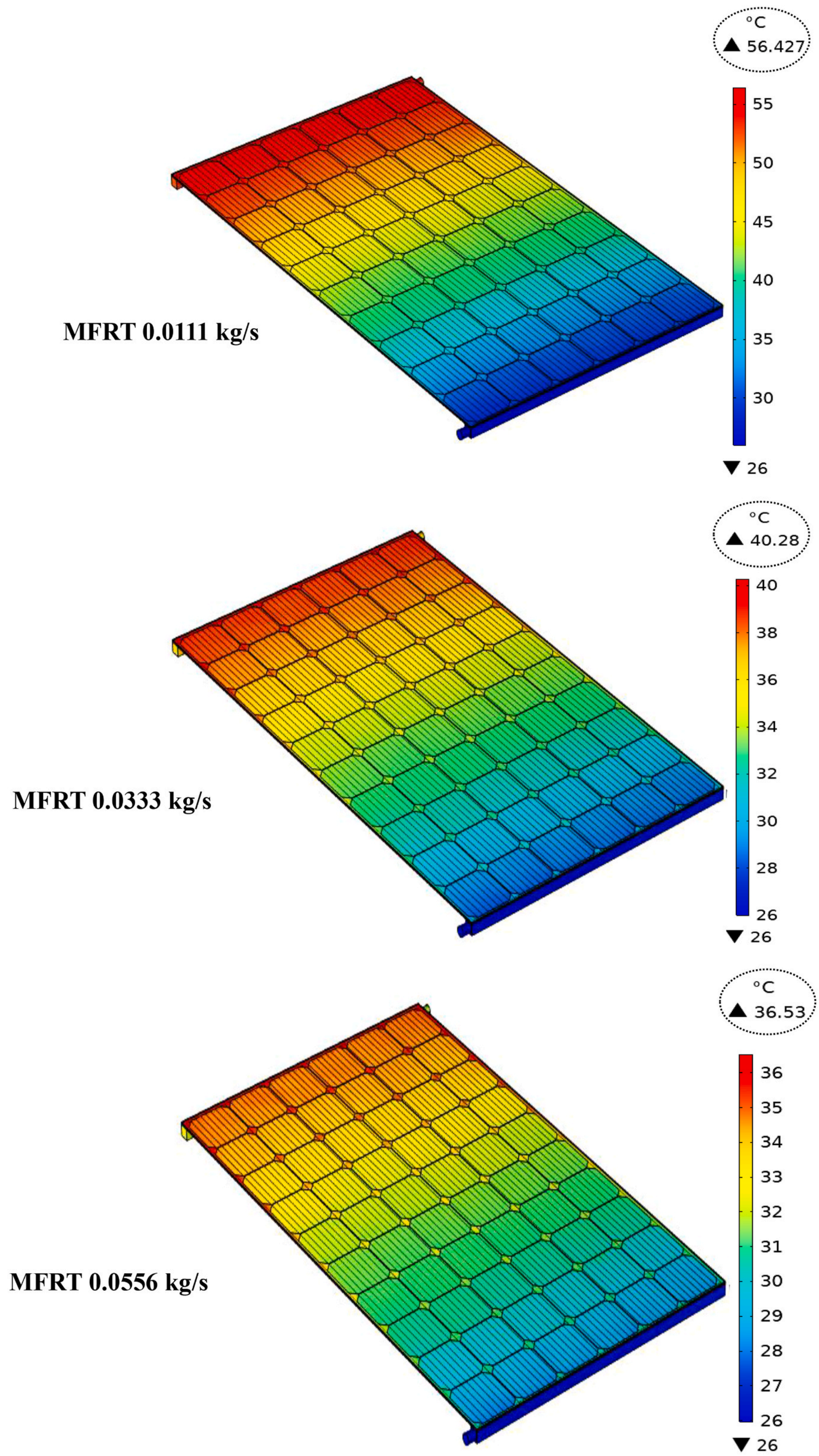

Fig. 16. PV cell temperature of the PVT-S cooled by Cu/water nanofluid at G = 1000 W/m^2 for different MFRTs (0.0111, 0.0333, and 0.0556 kg/s).

irreversibility, while entropy generation reflects the increase in disorder and the degradation of energy available to perform work. Table 9 illustrates the effect of solar irradiance on exergy destruction and entropy generation for different systems, namely an uncooled PV-M, a water-cooled PVT-S, and a PVT-S using Cu/water nanofluid. We can see that exergy destruction increases with irradiance, rising from 206.105 W to 1268.354 W for the uncooled PV, from 204.827 W to 1222.153 W for PVT-S with Cu/water, and from 204.855 W to 1223.157 W for PVT-S with water when irradiance varies from 200 to 1200 W/m^2. This change can be explained by the increase in cell and fluid temperature, which accentuates thermal gradients and irreversible losses. The difference between the three systems is mainly due to the cooling effect, with the PVT-S, whether water or Cu/water nanofluid, maintaining lower temperatures in the cells and fluid, thereby reducing exergy losses

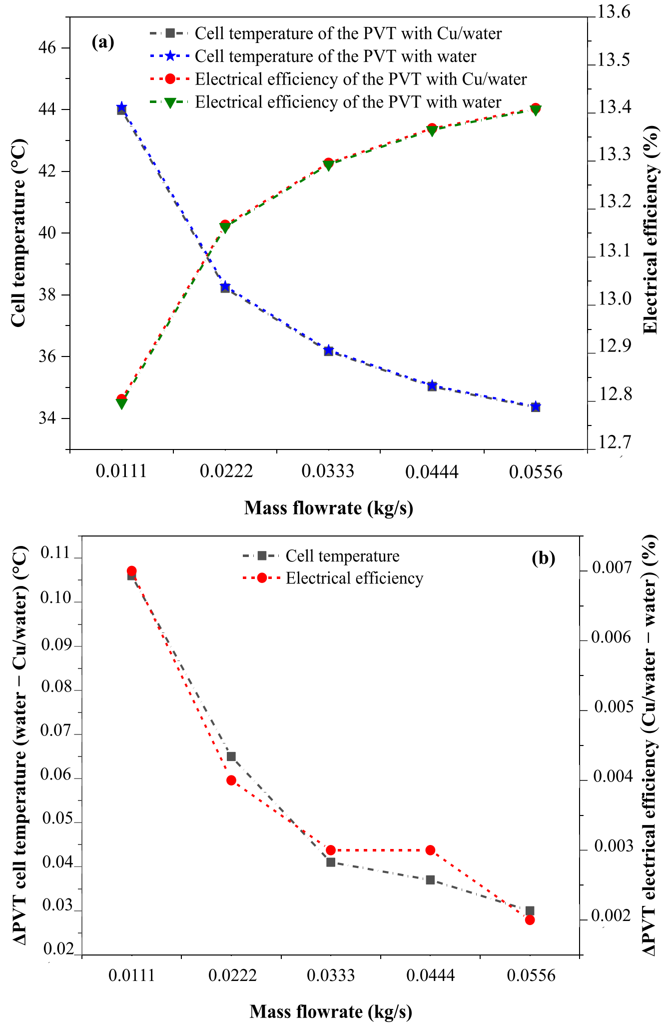

Fig. 17. Impact of heat-transfer fluid type (water and Cu/water nanofluid) and MFRTs (0.0111–0.0556 kg/s) on (a) PV cell temperature and EEF, and (b) the difference in PV cell temperature and EEF between the two fluids.

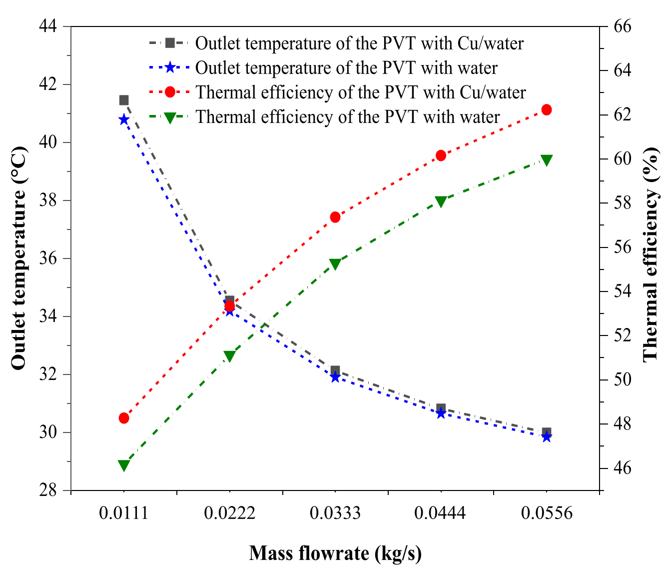

Fig. 18. Impact of heat-transfer fluid type (water and Cu/water nanofluid) and MFRTs (0.0111–0.0556 kg/s) on outlet fluid temperature and TEF.

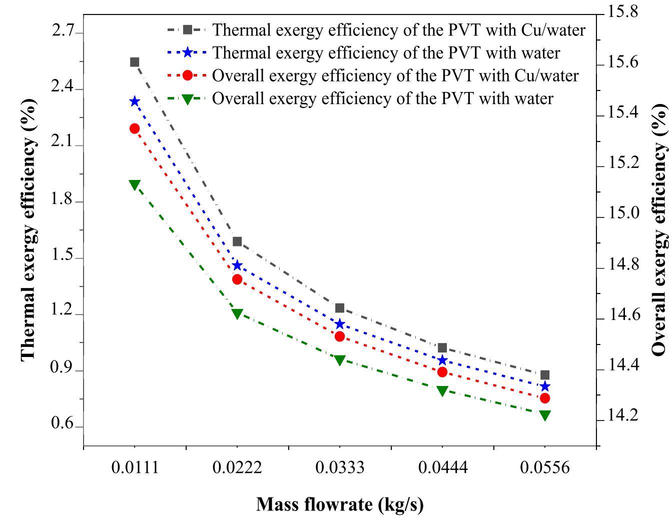

Fig. 19. Variation of thermal exergy and overall exergy efficiency of the PVT-S with MFRTs (0.0111–0.0556 kg/s) for the two heat-transfer fluids (water and Cu/water nanofluid).

Table 9
Variation in exergy destruction and entropy generation as a function of solar irradiance for PV and PVT-Ss using different cooling fluids.

G (W/m^2)	Uncooled PV-M		PVT-S with Cu/water		PVT-S with water	
	$\dot{X}_{less}$ (W)	$\dot{S}_{gen}$ (W/K)	$\dot{X}_{less}$ (W)	$\dot{S}_{gen}$ (W/K)	$\dot{X}_{less}$ (W)	$\dot{S}_{gen}$ (W/K)
200	206.105	0.6889	204.827	0.6846	204.855	0.6847
400	414.485	1.3855	409.458	1.3687	409.567	1.3691
600	625.013	2.0892	613.729	2.0515	613.979	2.0524
800	837.57	2.7998	817.452	2.7325	817.925	2.7341
1000	1052.045	3.5167	1020.407	3.4110	1021.158	3.4135
1200	1268.354	4.2398	1222.153	4.0854	1223.157	4.0887

compared to uncooled PV. Cu/water nanofluid offers a slight advantage over water alone due to its higher thermal conductivity, which promotes more efficient heat transfer and limits local thermal gradients. Similarly, entropy generation increases with irradiance, ranging from 0.6889 W/K to 4.2398 W/K for the uncooled PV, from 0.6846 W/K to 4.0854 W/K for the PVT-S with Cu/water, and from 0.6847 W/K to 4.0887 W/K for the PVT-S with water. This increase is linked to the intensification of thermal irreversibility as the amount of heat absorbed by the system increases.

Table 10 displays the evolution of exergy reduction and entropy creation due to various MFRT. Enhancing MFRT of water or Cu/water nanofluid increases exergy destruction, reflecting the intensification of irreversibility in system. A higher MFRT increases the energy flux transported, which amplifies thermal gradients and, consequently, exergy losses. The maximum values of exergy demolition and entropy creation are observed at the highest MFRT of 0.0556 kg/s, reaching 1021.158 W and 3.4135 W/K for the water-cooled PVT-S, and 1020.407

Table 10
Influence of MFRT on exergy destruction and entropy generation in PVT-Ss cooled with water and Cu/water nanofluid.

MFRT (kg/s)	PVT-S with Cu/water		PVT-S with water	
	$\dot{X}_{less}$ (W)	$\dot{S}_{gen}$ (W/K)	$\dot{X}_{less}$ (W)	$\dot{S}_{gen}$ (W/K)
0.0111	1007.762	3.3687	1010.347	3.3773
0.0222	1014.834	3.3923	1016.394	3.3976
0.0333	1017.514	3.4013	1018.579	3.4049
0.0444	1019.184	3.4069	1020.019	3.4097
0.0556	1020.407	3.4110	1021.158	3.4135

W and 3.4110 W/K for the PVT-S with Cu/water nanofluid.

3.6. Annual energy production analysis

The annual energy and exergy production of PV-M and PVT-Ss was analyzed to examine their economic viability. Two heat transfer fluids were considered, namely water and Cu/water nanofluid, considering the average daily solar radiation characteristic of the city of El Jadida, Morocco. Based on equations (32)–(34), the performance of a conventional PV-M and two PVT-S configurations (cooled with water and Cu/water nanofluid) was quantified for the first year of production and after twenty years of operation, allowing the effects of aging and cumulative losses to be considered. The results, presented in Table 11, confirm the clear superiority of PVT-Ss over PV-Ms alone. In the first year, annual energy production reached 2,672,093 kWh for the PVT-S with Cu/water nanofluid and 2,592,417 kWh for the water-cooled module, compared to only 438,888 kWh for the uncooled PV-M. After twenty years, these values decrease to 2293.894 kWh, 2225.495 kWh, and 376.769 kWh, respectively. This reduction is attributed to the combined effect of component wear and tear and the gradual decline in PV cell performance over time. The exergy analysis follows a similar trend, although the variation is more moderate. The PVT-S exergy production with nanofluid decreases from 515.76 kWh in the first year to 442.761 kWh after twenty years, while that of the PVT-S with water decreases from 513.94 kWh to 441.199 kWh over the same period. These results highlight that the use of a heat transfer fluid not only improves heat extraction but also the overall efficiency of the system by maintaining a lower operating temperature for the PV cells. The PVT-S using Cu/water nanofluid stands out as the most efficient configuration, thanks to its ability to ensure better thermal stability and simultaneously optimize energy and exergy yields. In addition, the operating time has a decisive influence on the performance of the systems studied.

3.7. Sustainability analysis

Analysis of the sustainability index shows that both MFRT and solar irradiance influence the sustainability of PVT-Ss. Fig. 20a shows that increasing the MFRT results in a slight decrease in the sustainability index for both configurations. The index decreases from 1.1783 to 1.1658 for the water system, and for the Cu/water nanofluid system, it decreases from 1.1813 to 1.1666 due to increasing MFRT (0.0111–0.0556 kg/s). This reduction is explained by increased heat losses and irreversibility at higher flow rates, which limit the system's overall efficiency. The difference between the two fluids is due to the higher thermal conductivity of the Cu/water nanofluid, which allows for better heat extraction and slightly mitigates the decrease in sustainability. In contrast, Fig. 20b illustrates that the durability index increases with solar irradiance. The water system rises from 1.1622 to 1.1679, and the Cu/water system from 1.1624 to 1.1689 when the irradiance varies from 200 to 1200 W/m^2. This positive trend results from improved energy and heat production under higher irradiance levels, which reduces the relative thermal load and promotes more sustainable operation of the system.

3.8. Performance comparison with previous studies

This section presents a comparison between the system studied and work already published in the literature. Table 12 highlights the overall energy and exergy efficiency of a PVT-S using Cu/water nanofluids, compared to values reported in the literature. The superiority of the total energy efficiency of the proposed system (78.31 %) can be explained by the synergistic combination of the new micro-heat exchanger, which ensures uniform cooling, and the use of Blade-type nanoparticles with a high form factor, optimizing thermal conductivity and heat transfer coefficients.

Table 13 presents a comparison of the maximum pressure reached in the system studied with that of PVT-Ss in the literature. This comparison shows that the proposed system has minimal pressure drop, whereas previous studies report pressure drops ranging from 300 to 874 Pa, despite using much lower MFRTs (0.00136–0.00556 kg/s) compared to the high MFRT of the system under study (0.0556 kg/s). This increase in pressure drop in existing systems forces the pump to work harder to maintain the desired flow rate, resulting in higher power consumption and thus a decrease in the overall efficiency of the system. In practical applications, this overconsumption can increase operating costs and limit the actual energy efficiency of the PVT-S, particularly when the fluid flow rate is low and the pump must operate at more constrained speeds to compensate for significant pressure losses. These results confirm that the new micro-heat exchanger offers high thermal performance while maintaining low pressure drops, outperforming the PVT-Ss studied in the literature, even at significantly higher flow rates.

4. Conclusions

This study analyzed a new P PVT-S, whose performance was evaluated using three-dimensional numerical modeling performed in COMSOL Multiphysics. The approach adopted allowed for an in-depth examination of several aspects based on variations in irradiance and MFRT, including energy performance, durability, exergy efficiency, annual production, exergy destruction, and entropy generation. Two heat transfer fluids, namely pure water and Cu/water nanofluid, were considered to compare their cooling capacity and impact on the system's overall efficiency. In addition, the influence of different Cu nanoparticle forms was studied to identify the most efficient configuration. The simulations were conducted based on solar irradiance and various MFRTs.

The main results obtained in this research can be summarized as follows.

- ❖ The shape of nanoparticles is a key parameter in improving the performance of PVT-Ss. The blade geometry of Cu nanoparticles proves to be the most effective, with a 3.21 % improvement in TEF compared to the octahedron shape, and a 3.56 % improvement compared to water cooling, under an irradiance of 1000 W/m^2.
- ❖ The increase in solar radiation raises the temperature of the cells to 36.071 °C for PVT-S water, 36.016 °C for PVT-S Cu/water, and 69.148 °C for PV-M, reducing EEFs to 13.302 %, 13.305 %, and 11.218 %, while improving TEFs to 63.059 % and 65.011 %. Meanwhile, increasing the MFRT reduces the temperature of the cells

Table 11
Annual energy and exergy production of PV-M and PVT-Ss (water and Cu/water nanofluid) for the 1st and 20th years of operation.

Production year considered	System Type	$E_{ele,ann}$ (kWh)	$E_{th,ann}$ (kWh)	$E_{ntot,ann}$ (kWh)	$Ex_{ele,ann}$ (kWh)	$Ex_{th,ann}$ (kWh)	$Ex_{tot,ann}$ (kWh)
t = 1	PVT-S with Cu/water	491.993	2180.100	2672.093	491.993	23.767	515.76
	PVT-S with water	491.883	2100.534	2592.417	491.883	22.057	513.94
	Uncooled PV-M	438.888	0	438.888	438.888	0	438.888
t = 20	PVT-S with Cu/water	422.358	1871.536	2293.894	422.358	20.403	442.761
	PVT-S with water	422.264	1803.231	2225.495	422.264	18.935	441.199
	Uncooled PV-M	376.769	0	376.769	376.769	0	376.769

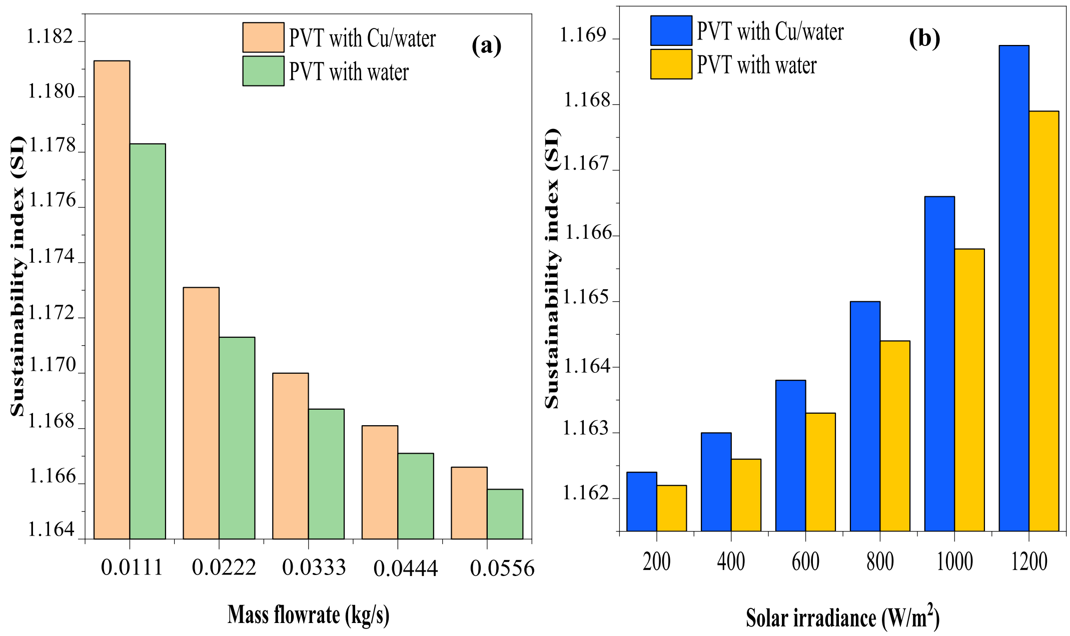

Fig. 20. Sustainability index of the PVT-Ss under different operating conditions: (a) variation with MFRT (0.0111–0.0556 kg/s) and (b) variation with solar irradiance (200–1000 W/m^2) for water and Cu/water nanofluid.

Table 12
Comparison of the total energy and exergy efficiency of PVT-Ss using Cu/water nanofluid with studies in the literature.

References &year	Study type	Concentration (%)	Fluid type	η_{Total} (%)	ε_{PVT} (%)
Alsharifi et al. [66], 2024	Numerical	–	Water	74.96	15.38
Alktranee et al. [59], 2024	Experimental	0.3	CuO/ water	49.2	10.91
Alktranee et al. [59], 2024	Experimental	0.2	TiO_2-Fe_2O_3/ water	54.22	14.11
Sreekumar et al. [67], 2024	Experimental	0.1	MXene/ C-dot	75.36	20.68
Hosseinzadeh et al. [68], 2018	Experimental	0.2	ZnO/ water	65.71	13.61
Göksu and Oztop. [69], 2025	Numerical	–	Water	53.45	15.47
Sardarabadi et al. [70], 2017	Experimental	0.2	TiO_2/ water	57.97	11.93
Present study	Numerical	2	Cu/ water	78.31	14.28

Table 13
Analysis of PVT system pressure drop compared to the literature.

Reference	Year	Absorber type	Pressure value	Inlet MFRT or velocity
Poredoš et al. [71]	2020	Bionic Parallel	385 Pa 778 Pa	0.5 m/s
Olmuş et al. [53]	2025	Serpentine	789.892 Pa	0.00556 kg/s
Kazemian et al. [29]	2024	Spiral	300–400 Pa	0.00136 kg/s
Present study	2025	Two-sided serpentine Heat exchanger with 49 microchannels	874 Pa 264.93 Pa	0.0556 kg/s

and slightly increases EEF to 13.408 % for PVT-S water and 13.410 % for PVT-S Cu/water.

- ❖ The total exergy efficiency increases with irradiance, reaching 14.381 % for water-cooled PVT-S and 14.451 % for Cu/water-cooled PVT-S, while it decreases with increasing MFRT, reaching maximum values of 15.133 % and 15.35 % at the lowest MFRT.
- ❖ Exergy destruction and entropy generation increase with irradiance, reaching 1222.153 W and 4.0854 W/K for Cu/water PVT-S, 1223.157 W and 4.0887 W/K for water PVT-S, and 1268.354 W and 4.2398 W/K for PV-M, and also increase with increasing MFRT.
- ❖ The PVT-S Cu/water system has the highest annual energy (2672.093 kWh) and annual exergy (515.76 kWh) among the systems studied, with durability increasing with irradiance (1.1689 for Cu/water, 1.1679 for water) but decreasing slightly when the MFRT is higher, reaching 1.1813 and 1.1783, respectively, at the lowest MFRT.

5. Future research directions

For future work, it is recommended that the PVT-S studied be built experimentally to confirm the numerical results obtained, while exploring the use of different nanofluids, single or hybrid, to maximize thermal and electrical performance. Optimizing the collector design, including channel geometry, spacing, and materials, as well as studying the system's behavior under various climatic conditions and seasons, could improve overall energy efficiency. In addition, integrating PVT-S with thermal or electrical storage systems and developing active real-time control strategies would allow operation to be adapted to irradiance and energy demand. Comprehensive economic and environmental analyses and assessments of the long-term durability and reliability of materials are essential to ensure the industrial applicability of the system. Finally, exploring innovative coatings and advanced nanomaterials to reduce heat loss and homogenize cell temperature could further enhance the system's performance and longevity.

CRediT authorship contribution statement

Yassine El Alami: Writing – original draft, Visualization, Validation, Software, Methodology, Investigation, Formal analysis, Data curation, Conceptualization. **Elhadi Baghaz:** Writing – review & editing, Visualization, Supervision, Funding acquisition. **Mohamed Errebii:** Writing – review & editing, Visualization, Investigation, Data curation. **Rehena Nasrin:** Writing – review & editing, Validation, Methodology, Investigation. **Mohamed El Habib Amagour:** Writing – review & editing, Investigation, Data curation. **Khaled M. Al-Aribe:** Writing – review & editing, Formal analysis, Conceptualization. **Adnan Ibrahim:** Writing – review & editing, Investigation, Formal analysis, Data curation, Conceptualization.

Funding declaration

This research received no specific grant from any funding agency in the public, commercial, or not-for-profit sectors.

Declaration of competing interest

The authors declare that they have no known competing financial interests or personal relationships that could have appeared to influence the work reported in this paper.

Data availability

The datasets used and/or analyzed during the current study available from the corresponding author on reasonable request.

References

[1] Madadi M, Abbasian Arani AA. Experimental evaluation of photovoltaic thermal (PVT) system using a modular heat collector with flat back shape fins, pipe, nanofluids and phase change material. Sol Energy Mater Sol Cells 2025;280:113294. https://doi.org/10.1016/j.solmat.2024.113294.

[2] El Alami Y, Zohal B, Nasrin R, Benhmida M, Faize A, Baghaz E. Solar thermal, photovoltaic, photovoltaic thermal, and photovoltaic thermal phase change material systems: a comprehensive reference guide. Int Commun Heat Mass Tran 2024;159:108135. https://doi.org/10.1016/j.icheatmasstransfer.2024.108135.

[3] El Alami Y, Baghaz E, Nasrin R, Al-Damook M, Bendaoud R, Bouragba T, et al. Up-to-Date review on flat-plate solar hybrid photovoltaic thermal systems: absorber designs and fabrication materials. Int J Energy Res 2025;2025:5547555. https://doi.org/10.1155/er/5547555.

[4] Ebaid MunzerSY, Ghrair AyoupM, Al-Busoul M. Experimental investigation of cooling photovoltaic (PV) panels using (TiO2) nanofluid in water -polyethylene glycol mixture and (Al2O3) nanofluid in water- cetyltrimethylammonium bromide mixture. Energy Convers Manag 2018;155:324–43. https://doi.org/10.1016/j.enconman.2017.10.074.

[5] Jabeen N, Waqas A, Ali M. Dynamic performance evaluation of PCM-based PVT systems: combined impact of design modifications and nanofluids. J Energy Storage 2025;121:116645. https://doi.org/10.1016/j.est.2025.116645.

[6] Alqatamin A, Jinzhan S. Numerical analysis and design of photovoltaic-thermal (PVT) system with novel water-cooling channel structure integrated with perforated V-shape fins. Renew Energy 2025;243:122587. https://doi.org/10.1016/j.renene.2025.122587.

[7] Variyenli Hİ, Yousefi M, Tuncer AD, Sözen A, Göksel BÇ, Khanlari A. Numerical and experimental analysis of a water cooled photovoltaic-thermal system using modified tubes. Appl Therm Eng 2025;279:127559. https://doi.org/10.1016/j.applthermaleng.2025.127559.

[8] El Alami Y, Achouby HE, Baghaz E, Hajjaj C, Nasrin R. An innovative photovoltaic thermal system with direct water-cell contact: energy, exergy, and sustainability analysis. Sol Energy 2025;300:113827. https://doi.org/10.1016/j.solener.2025.113827.

[9] Satpute J, Srinidhi C, Rathore SS, Yadav SM, Kumar A, Gajbhiye A, et al. Parametric influence and efficiency assessment of water-cooled photovoltaic thermal PV/T absorber designs. Energy 2025;320:135218. https://doi.org/10.1016/j.energy.2025.135218.

[10] Wang Z, Hou G, Taherian H, Song Y. Numerical investigation of innovative photovoltaic–thermal (PVT) collector designs for electrical and thermal enhancement. Energies 2024;17:2429. https://doi.org/10.3390/en17102429.

[11] Jha P, Das B, Gupta R, Kumar N. An experimental analysis of photovoltaic thermal collector with trapezoidal and plain plates: an energy, exergy, and life cycle assessment. Appl Therm Eng 2025;274:126769. https://doi.org/10.1016/j.applthermaleng.2025.126769.

[12] Alami YE, Baghaz E, Nasrin R, Padmanaban S, Louzazni M. Numerical approach of an advanced hybrid photovoltaic thermal system based on exergy, energy, enviro-economic, and sustainability factors. Results Eng 2025:106342. https://doi.org/10.1016/j.rineng.2025.106342.

[13] Basalike P, Wang P, Zhang J, Ahmad R. Numerical investigation on the performance characteristics and sustainability of dual function roll bond photovoltaic thermal unit integrating a novel channel. Sol Energy Mater Sol Cells 2024;276:113045. https://doi.org/10.1016/j.solmat.2024.113045.

[14] Liu H, Feng X, Zhao D, Wang T, Li X. Numerical simulation and optimization of bionic leaf-vein structure collector performance in photovoltaic-thermal system. Appl Therm Eng 2025;280:127883. https://doi.org/10.1016/j.applthermaleng.2025.127883.

[15] Kumar V, Singh UR, Bhogilla SS. Experimental investigation of an innovative PV/T collector in jammu climatic conditions. Therm Sci Eng Prog 2025;59:103312. https://doi.org/10.1016/j.tsep.2025.103312.

[16] Almadhhachi M, Ajeena AM, Al-Madhhachi HS, Farkas I. Numerical analysis of the effects of transparent thermal materials in photovoltaic thermal systems. Results Eng 2025;26:105582. https://doi.org/10.1016/j.rineng.2025.105582.

[17] El Alami Y, Baghaz E, Nasrin R, Chanaa F, Bendaoud R, Padmanaban S, et al. Experimental-numerical comparative study of performance and cost-effectiveness of partially- and fully-cooled photovoltaic thermal systems. Case Stud Therm Eng 2025;73:106660. https://doi.org/10.1016/j.csite.2025.106660.

[18] Çerçi KN. Energy, exergy, economic and enviro-economic analysis and artificial neural network modeling of an air-cooled PVT collector with NACA 8412 airfoils. Appl Therm Eng 2025;277:126955. https://doi.org/10.1016/j.applthermaleng.2025.126955.

[19] Safarianbana B, Dashtbozorg A, Shanbedi M. Enhancing PV/T system efficiency with MAX phase/water nanofluids: experimental insights into optimal cooling strategies. Energy 2025;340:139223. https://doi.org/10.1016/j.energy.2025.139223.

[20] Sofiah AGN, Samykano M, Rajamony RK, Pasupuleti J, Pandey AK, Sulaiman NF. Cutting-edge heat transfer: how hexagonal boron nitride nanofluids boost solar photovoltaic thermal (PVT) system performance? Renew Energy 2025;252:123501. https://doi.org/10.1016/j.renene.2025.123501.

[21] Radhi FA, Ibrahim A, Azeez HL, Fazlizan A, Sopian K, Ali AA, et al. Experimental analysis of a photovoltaic thermal collector utilizing a novel spring insert in a micro-fin absorber tube with twisted tape, nanofluid, and nanophase change material integration. Appl Therm Eng 2025;269:126128. https://doi.org/10.1016/j.applthermaleng.2025.126128.

[22] Azeez HL, Ibrahim A, Ahmed BO, Dol SS, Al-Waeli AHA, Jaber M. Experimental investigations of heat transfer, energy, and exergy-based sustainability of a novel photovoltaic thermal system. Case Stud Therm Eng 2025;70:106089. https://doi.org/10.1016/j.csite.2025.106089.

[23] Jaber M, Ibrahim A, Azeez HL, Ahmed BO, Ud Din SI, Jarimi H. Electrical and thermal analysis of a newly designed photovoltaic thermal collector featuring inner and outer micro-fin surface tube with broken double V-cuts twisted tapes: an experimental study. Appl Therm Eng 2025;274:126757. https://doi.org/10.1016/j.applthermaleng.2025.126757.

[24] Prasetyo SD, Arifin Z, Prabowo AR, Budiana EP. Investigation of the addition of fins in the collector of water/Al2O3-based PV/T system: validation of 3D CFD with experimental study. Case Stud Therm Eng 2024;60:104682. https://doi.org/10.1016/j.csite.2024.104682.

[25] Alsharifi T, Sultan Aljibori HS, Mahdi JM. Design optimization and performance evaluation of a photovoltaic/thermal collector with porous twisted tape inserts: a comprehensive energy and exergy analysis. Int Commun Heat Mass Tran 2024;159:108104. https://doi.org/10.1016/j.icheatmasstransfer.2024.108104.

[26] El Alami Y, Ameur A, Benhmida M, Rabhi A, Baghaz E. Performance evaluation of different new channel box photovoltaic thermal systems. J Clean Prod 2024;478:143953. https://doi.org/10.1016/j.jclepro.2024.143953.

[27] Du Y, Tao W, Liu Y, Jiang J, Huang H. Heat transfer modeling and temperature experiments of crystalline silicon photovoltaic modules. Sol Energy 2017;146:257–63. https://doi.org/10.1016/j.solener.2017.02.049.

[28] Jones AD, Underwood CP. A thermal model for photovoltaic systems. Sol Energy 2001;70:349–59. https://doi.org/10.1016/S0038-092X(00)00149-3.

[29] Kazemian A, Ma T, Hongxing Y. Evaluation of various collector configurations for a photovoltaic thermal system to achieve high performance, low cost, and lightweight. Appl Energy 2024;357:122422. https://doi.org/10.1016/j.apenergy.2023.122422.

[30] Alami YE, Dahmani H, Ouerradi F, Zohal B, Bendaoud R, Baghaz E. Impact of heat exchanger materials on the performance of solar hybrid photovoltaic thermal (PVT) systems: 3D analysis. In: Hajji B, Gagliano A, Mellit A, Rabhi A, Calì M, editors. Proc. 4th int. Conf. Electron. Eng. Renew. Energy syst., vol. 2. Singapore: Springer Nature; 2025. p. 609–19. https://doi.org/10.1007/978-981-97-9975-6_58.

[31] Alami YE, Lamkaddem A, Bendaoud R, Talbi S, Louzazni M, Baghaz E. Numerical study of a water-based photovoltaic-thermal (PVT) hybrid solar collector with a new heat exchanger. E-Prime - Adv Electr Eng Electron Energy 2024:100693. https://doi.org/10.1016/j.prime.2024.100693.

[32] Nasrin R, Hasanuzzaman M, Rahim NA. Effect of high irradiation on photovoltaic power and energy. Int J Energy Res 2018;42:1115–31. https://doi.org/10.1002/er.3907.

[33] Nahar A, Hasanuzzaman M, Rahim NA. Numerical and experimental investigation on the performance of a photovoltaic thermal collector with parallel plate flow channel under different operating conditions in Malaysia. Sol Energy 2017;144:517–28. https://doi.org/10.1016/j.solener.2017.01.041.

[34] Nasrin R. Water/MWCNT nanofluid based cooling system of PVT: experimental and numerical research. Renew Energy 2018;121:286–300. https://doi.org/10.1016/j.renene.2018.01.014.

[35] Alami YE, Baghaz E, Nasrin R, Haboubi K, Benhmida M, Ibrahim A. Integrated sustainability and 4E analysis of hybrid nanofluid featured PVT systems incorporating diverse backsheets. Appl Therm Eng 2025:129147. https://doi.org/10.1016/j.applthermaleng.2025.129147.

[36] Büyükalaca O, Kılıç HM, Olmuş U, Güzelel YE, Çerçi KN. Numerical investigation and ANN modeling of performance for hexagonal boron Nitride-water nanofluid PVT collectors. Therm Sci Eng Prog 2023;43:101997. https://doi.org/10.1016/j.tsep.2023.101997.

[37] El Alami Y, Baghaz E, Bendaoud R, Chanaa F, Benhmida M, Ezzaki H, et al. Experimental-numerical investigation of the photovoltaic thermal system with polypropylene heat exchanger: case in Morocco. IET Renew Power Gener 2025;19:e70041. https://doi.org/10.1049/rpg2.70041.

[38] Kazemian A, Salari A, Ma T. A year-round study of a photovoltaic thermal system integrated with phase change material in shanghai using transient model. Energy Convers Manag 2020;210:112657. https://doi.org/10.1016/j.enconman.2020.112657.

[39] Kazemian A, Salari A, Hakkaki-Fard A, Ma T. Numerical investigation and parametric analysis of a photovoltaic thermal system integrated with phase change material. Appl Energy 2019;238:734–46. https://doi.org/10.1016/j.apenergy.2019.01.103.

[40] Ahmadinejad M, Soleimani A, Gerami A. The effects of a novel baffle-based collector on the performance of a photovoltaic/thermal system using SWCNT/water nanofluid. Therm Sci Eng Prog 2022;34:101443. https://doi.org/10.1016/j.tsep.2022.101443.

[41] Lee Y, Tay AAO. Finite element thermal analysis of a solar photovoltaic module. Energy Proc 2012;15:413–20. https://doi.org/10.1016/j.egypro.2012.02.050.

[42] Herrando M, Ramos A, Zabalza I, Markides CN. A comprehensive assessment of alternative absorber-exchanger designs for hybrid PVT-Water collectors. Appl Energy 2019;235:1583–602. https://doi.org/10.1016/j.apenergy.2018.11.024.

[43] Fayaz H, Rahim NA, Hasanuzzaman M, Rivai A, Nasrin R. Numerical and outdoor real time experimental investigation of performance of PCM based PVT system. Sol Energy 2019;179:135–50. https://doi.org/10.1016/j.solener.2018.12.057.

[44] Nahar A, Hasanuzzaman M, Rahim NA. A three-dimensional comprehensive numerical investigation of different operating parameters on the performance of a photovoltaic thermal system with pancake collector. J Sol Energy Eng 2017;139:031009. https://doi.org/10.1115/1.4035818.

[45] Nasrin R, Hasanuzzaman M, Rahim NA. Effect of high irradiation and cooling on power, energy and performance of a PVT system. Renew Energy 2018;116:552–69. https://doi.org/10.1016/j.renene.2017.10.004.

[46] Dubey S, Tay AAO. Testing of two different types of photovoltaic–thermal (PVT) modules with heat flow pattern under tropical climatic conditions. Energy Sustain Dev 2013;17:1–12. https://doi.org/10.1016/j.esd.2012.09.001.

[47] Alami YE, Baghaz E, Nasrin R, Hajjaj C, Benhmida M, Al-Aribe KM, et al. Numerical exploration and relational impact ranking of critical parameters in 3D PV module studies. Results Eng 2025:107097. https://doi.org/10.1016/j.rineng.2025.107097.

[48] El Alami Y, Rami M, Hajjaj C, Benhmida M, Faize A, Baghaz E. Three-dimensional thermal modeling and analysis of the heat source, the impact of encapsulation materials and the back sheet of silicon PV modules. Appl Therm Eng 2025;280:128430. https://doi.org/10.1016/j.applthermaleng.2025.128430.

[49] Hissouf M, Feddaoui M, Najim M, Charef A. Numerical study of a covered photovoltaic-thermal Collector (PVT) enhancement using nanofluids. Sol Energy 2020;199:115–27. https://doi.org/10.1016/j.solener.2020.01.083.

[50] El Hadi Attia M, Zayed ME, Kabeel AE, Khelifa A, Irshad K, Rehman S. Numerical analysis and design of a novel solar photovoltaic thermal system using finned cooling channel structures embedded with air/TiO2–water nano bi-fluid. Sol Energy 2024;269:112368. https://doi.org/10.1016/j.solener.2024.112368.

[51] Alazwari MA, Basem A, AL-bonsrulah HAZ, Almitani KH, Abu-Hamdeh NH, Albdeiri MS, et al. Assessment of photovoltaic system in existence of nanomaterial cooling flow. Results Eng 2024;24:103264. https://doi.org/10.1016/j.rineng.2024.103264.

[52] Akbar AA, Ahammad NA, Awan AU, Hussein AK, Gamaoun F, Tag-ElDin EM, et al. Insight into the role of nanoparticles shape factors and diameter on the dynamics of rotating water-based fluid. Nanomaterials 2022;12:2801. https://doi.org/10.3390/nano12162801.

[53] Olmuş U, Güzelel YE, Çerçi KN, Büyükalaca O. Numerical analysis and comparison of different serpentine-based photovoltaic-thermal collectors. Renew Energy 2025;241:122196. https://doi.org/10.1016/j.renene.2024.122196.

[54] Azad AK, Parvin S. Photovoltaic thermal (PV/T) performance analysis for different flow regimes: a comparative numerical study. Int J Thermofluids 2023;18:100319. https://doi.org/10.1016/j.ijft.2023.100319.

[55] Alami YE, Ouerradi F, Bounouar S, Benhmida M, Rhiat M, Benhala B, et al. Comparative study of the performance of photovoltaic and photovoltaic thermal solar systems: case study in El Jadida. E3S Web Conf 2025;601:00011. https://doi.org/10.1051/e3sconf/202560100011.

[56] Abbas S, Zhou J, Hassan A, Yuan Y, Yousuf S, Sun Y, et al. Economic evaluation and annual performance analysis of a novel series-coupled PV/T and solar TC with solar direct expansion heat pump system: an experimental and numerical study. Renew Energy 2023;204:400–20. https://doi.org/10.1016/j.renene.2023.01.032.

[57] Kalogirou SA, Karellas S, Braimakis K, Stanciu C, Badescu V. Exergy analysis of solar thermal collectors and processes. Prog Energy Combust Sci 2016;56:106–37. https://doi.org/10.1016/j.pecs.2016.05.002.

[58] Khelifa A, Abdelgaied M, Attia MEH, Harby K, Arıcı M. Development and optimization of dual-objective PVT modules for a smart residential building using inclined fins. J Build Eng 2024;97:110893. https://doi.org/10.1016/j.jobe.2024.110893.

[59] Alktranee M, Al-Yasiri Q, Shehab MA, Bencs P, Németh Z, Hernadi K. Experimental and numerical study of a photovoltaic/thermal system cooled by metal oxide nanofluids. Alex Eng J 2024;94:55–67. https://doi.org/10.1016/j.aej.2024.03.050.

[60] Alktranee M, Al-Yasiri Q, Al-Furaiji MA, Al-Hamzawi HAH, Bencs P, Szabó M. Performance improvement of flat plate solar collector employing phase change material bags and hybrid nanofluid. Results Eng 2025;27:106972. https://doi.org/10.1016/j.rineng.2025.106972.

[61] Abdo S, Saidani-Scott H, Abdelrahman MA. Numerical study with eco-exergy analysis and sustainability assessment for a stand-alone nanofluid PV/T. Therm Sci Eng Prog 2021;24:100931. https://doi.org/10.1016/j.tsep.2021.100931.

[62] Azeez HL, Ibrahim A, Ahmed BO, Dol SS, Al-Waeli AHA, Jaber M. Experimental investigations of heat transfer, energy, and exergy-based sustainability of a novel photovoltaic thermal system. Case Stud Therm Eng 2025;70:106089. https://doi.org/10.1016/j.csite.2025.106089.

[63] Azeez HL, Ibrahim A, Ahmed BO, Kasprzak J, Al-Waeli AHA, Jaber M. 5E assessments of a novel solar collector under high cooling demand scenarios: experimental and sustainability studies. Energy 2025;326:136297. https://doi.org/10.1016/j.energy.2025.136297.

[64] Bisengimana E, Zhou J, Binama M, Yuan Y. Numerical investigation on the factors influencing the temperature distribution of photovoltaic/thermal (PVT) evaporator/condenser for heat pump systems. Renew Energy 2022;194:885–901. https://doi.org/10.1016/j.renene.2022.05.154.

[65] Attia MEH, Zayed ME, Kabeel AE, Khelifa A, Arıcı M, Abdelgaied M. Design and performance optimization of a novel zigzag channeled solar photovoltaic thermal system: numerical investigation and parametric analysis. J Clean Prod 2024;434:140220. https://doi.org/10.1016/j.jclepro.2023.140220.

[66] Alsharifi T, Mahdi JM, Togun H, Taqi Al-Najjar HM, Ben Khedher N, Cairns A, et al. Design and optimization of a household photovoltaic/thermal collector with serpentine tube: energy and exergy analysis. Appl Therm Eng 2024;246:122983. https://doi.org/10.1016/j.applthermaleng.2024.122983.

[67] Sreekumar S, Pugsley A, Chakrabarti S, Hewitt N, Mondol JD, Shah N. Experimental investigation on the performance of MXene/C-dot hybrid nanofluid-based photovoltaic/thermal system: an energy, Exergy, and enviro-economic analysis. Sol Energy Mater Sol Cells 2024;272:112904. https://doi.org/10.1016/j.solmat.2024.112904.

[68] Hosseinzadeh M, Sardarabadi M, Passandideh-Fard M. Energy and exergy analysis of nanofluid based photovoltaic thermal system integrated with phase change material. Energy 2018;147:636–47. https://doi.org/10.1016/j.energy.2018.01.073.

[69] Göksu TT, Öztop HF. Energy and exergy analysis of perforated twisted tapes: RSM-Driven optimization of geometrical parameters for PV/T systems. Appl Therm Eng 2025;279:127550. https://doi.org/10.1016/j.applthermaleng.2025.127550.

[70] Sardarabadi M, Hosseinzadeh M, Kazemian A, Passandideh-Fard M. Experimental investigation of the effects of using metal-oxides/water nanofluids on a photovoltaic thermal system (PVT) from energy and exergy viewpoints. Energy 2017;138:682–95. https://doi.org/10.1016/j.energy.2017.07.046.

[71] Poredoš P, Tomc U, Petelin N, Vidrih B, Flisar U, Kitanovski A. Numerical and experimental investigation of the energy and exergy performance of solar thermal, photovoltaic and photovoltaic-thermal modules based on roll-bond heat exchangers. Energy Convers Manag 2020;210:112674. https://doi.org/10.1016/j.enconman.2020.112674.